MANY BODY INTERACTIONS OF NEUTRAL AND CHARGED HYDROGEN BONDED CLUSTERS

by

Albert A. DeFusco III

B. S., Frostburg State University, 2003

Submitted to the Graduate Faculty of

the School of Arts and Sciences in partial fulfillment

of the requirements for the degree of

Doctor of Philosophy

University of Pittsburgh

2008

UNIVERSITY OF PITTSBURGH

SCHOOL OF ARTS AND SCIENCES

This dissertation was presented

by

Albert A. DeFusco III

It was defended on

June 11th 2008

and approved by

Kenneth D. Jordan, Department of Chemistry

Peter E. Siska, Department of Chemistry

David J. Earl, Department of Chemistry

Hyung J. Kim, Carnegie Mellon Department of Chemistry

Dissertation Director: Kenneth D. Jordan, Department of Chemistry

MANY BODY INTERACTIONS OF NEUTRAL AND CHARGED HYDROGEN BONDED CLUSTERS

Albert A. DeFusco III, PhD

University of Pittsburgh, 2008

Water clusters play a pivotal role in many chemical and biological processes. Understanding the molecular-level interactions between water molecules will greatly improve our understanding of these processes. Using high-level *ab initio* methods, a new classical force field model for water that accurately describes intermolecular interactions has been developed. This force field has been implemented as part of our Drude Model approach to study excess electron interactions with water clusters. The resulting potentials provide a description of $(H_2O)_n$ and $(H_2O)_n^-$ water clusters close to that obtained by much more computationally demanding high-level *ab initio* electronic structure calculations.

TABLE OF CONTENTS

LIST OF TABLES

LIST OF FIGURES

PREFACE

First, I thank Prof. Kenneth D. Jordan for his excellent mentorship. Five years is not long enough to learn all he has to teach.

To the members of the Jordan Group, I thank you for all your help and encouragement these last five years.

Finally, I thank my parents and three sisters for their tireless support of all my endeavors.

1.0 INTRODUCTION

Research into the nature of intermolecular interactions is one of the most important areas of theoretical chemistry. The strengths of intermolecular interactions are significantly smaller than the covalent bonds in molecules, and accurate calculations of such interaction energies has proven to be a computational challenge. In the traditional approach, the intermolecular energy between molecules A and B is computed as

$$E_{\text{int}} = E_{AB} - E_A - E_B, \tag{1.1}$$

where E_A and E_B are the energies of the isolated molecules A and B and E_{AB} is the total energy of the dimer, requires highly accurate energy evaluations of the three terms before subtraction. This approach is also prone to basis set superposition errors due to the use of incomplete basis sets.[1]

The supramolecular energy represented by equation 1.1 gives no insight about how two molecules interact. Perturbation theory approaches have become extremely popular to calculate chemically relevant contributions to the supramolecular energy.[2, 3] These interactions fall into four classes, electrostatic contributions between two unperturbed charge densities, induction of one charge density by the static field of another, dynamic correlation between two induced dipole moments, called dispersion, and exchange interactions arising from the indistinguishability of all the electrons in the system. Derivations of each of these interactions from perturbation theory will be presented below.

The zeroth-order hamiltonian of the system is the sum of the non-interacting hamiltonians of molecules A and B,

$$H^{(0)} = H_A + H_B, \tag{1.2}$$

with the zeroth-order wavefunction being the product of the ground state charge distributions of molecules A and B,

$$\Psi_0 = \Phi_0^A \Phi_0^B. \tag{1.3}$$

First order perturbation using the intermolecular operator $W_{A,B}$ gives rise to the following energy term,

$$E^{(1)} = \langle \Psi_0 | W_{A,B} | \Psi_0 \rangle. \tag{1.4}$$

Writing equation 1.4 in terms of one electron charge densities for molecules A and B and expanding the operator, $W_{A,B}$, in powers of the inverse intermolecular distance, R^{-1}, the electrostatic interaction for an arbitrary multipolar expansion of charge densities for molecules A and B is obtained,

$$E^{(1)} \approx T q^A q^B + T_\alpha \left(q^A \mu_\alpha^B - \mu_\alpha^A q^B \right) + \cdots, \tag{1.5}$$

where T is the electrostatic interaction between two point charges and T_α is the tensor for interaction between a point charge and a point dipole.[4] In equation 1.5, each molecular charge density has been expanded into classical moments about a single point, typically chosen to be the center of mass. In practice, the accuracy of equation 1.5 is highly dependent on the multipolar expansion. Some aspects of this will be discussed in the following chapter.

The second-order energy is given by

$$E^{(2)} = -\sum_{m \neq 0} \frac{|\langle \Psi_0 | W_{A,B} | \Psi_m \rangle|^2}{E_m - E_0}, \tag{1.6}$$

where Ψ_m are excited eigenfunctions of H_0. The induction energy at second-order is obtained when excitations Ψ_m are restricted to single excitations of the form $\Phi_n^A \Phi_0^B$ and $\Phi_0^A \Phi_n^B$, for single excitations of A and B respectively. With this constraint second-order energy is then written as

$$E_{\text{ind}}^{(2)} = -\sum_{n \neq 0} \frac{\left| \langle \Psi_0 | W_{A,B} | \Phi_n^A \Phi_0^B \rangle \right|^2}{E_n^A - E_0^A} - \sum_{n \neq 0} \frac{\left| \langle \Psi_0 | W_{A,B} | \Phi_0^A \Phi_n^B \rangle \right|^2}{E_n^B - E_0^B}. \tag{1.7}$$

The first term in equation 1.7 is the induction energy of the perturbed charge distribution A in the field of the unperturbed charge distribution B and *vice versa* for the second term.

Expanding the operator in powers of R^{-1} and integrating over the coordinates of molecule B, the left term becomes

$$E^A_{\text{ind}} = -\left(q^B T_\alpha - \mu^B_\beta T_{\alpha\beta} + \cdots\right) \sum_{n\neq 0} \frac{\langle\Psi_0|\hat{\mu}^A_\alpha|\Phi^A_n\Phi^B_0\rangle\langle\Phi^A_n\Phi^B_0|\hat{\mu}^A_{\alpha'}|\Psi_0\rangle}{E^A_n - E^A_0} \left(q^B T_{\alpha'} - \mu^B_{\beta'} T_{\alpha'\beta'} + \cdots\right). \tag{1.8}$$

Recognizing that the sum-over-states expression in the middle of equation 1.8 is the polarizability tensor, $\alpha^A_{\alpha\alpha'}/2$ of molecule A and that the multipole expansion is minus the electric field at charge distribution A due to charge distribution B ($\mathbf{F}^B_\alpha(A)$), the classical expression for the induction energy of charge distribution A is

$$E^A_{\text{ind}} = -\frac{1}{2}\mathbf{F}^B_\alpha(A)\mathbf{F}^B_{\alpha'}(A)\alpha^A_{\alpha\alpha'}. \tag{1.9}$$

The difference between the second-order energy in equation 1.6 and the induction energy of equation 1.7 is referred to as dispersion. This accounts for correlated motion of the electrons associated with the charge distributions A and B and is expressed with simultaneous excitations of each charge distribution, $\Phi^n_A\Phi^m_B$, with the energy being

$$E^{(2)}_{\text{disp}} = -\sum_{m\neq 0, n\neq 0} \frac{\left|\langle\Psi_0|W_{A,B}|\Phi^A_n\Phi^B_m\rangle\right|^2}{E^A_n + E^B_m - E^A_0 - E^B_0}. \tag{1.10}$$

Deriving an expression for the dispersion energy with separate contributions from A and B is difficult because equation 1.10 is not factorable. Using the Onsöld average-energy approximation,[5] London[6] showed that when the leading term in the multipole expansion in powers of R^{-1} is a product of the polarizabilities of the two charge distributions A and B

$$E_{\text{disp}} \approx -\frac{U_A U_B}{4(U_A + U_B)} \bar{\alpha}^A \bar{\alpha}^B T_{\alpha\beta} T_{\alpha\beta}, \tag{1.11}$$

where U_A and U_B are average excitation energies for A and B and $\bar{\alpha}^A$ and $\bar{\alpha}^B$ are average polarizabilities. In general, the orientationally averaged energy is expressed with a single parameter as $-C_6R^{-6}$ for molecular interactions. It should be noted that Casimir and Polder[7] presented another method to calculate the dispersion interaction which leads to an exact formula.

At this point it is worth noting that equation 1.3 ignores the indistinguishability of electrons in the two sub-systems, meaning Ψ_0 is not properly antisymmetric. The wavefunction should be expressed as $\mathcal{A}\Psi_0$ with the first-order energy given by

$$E_{HL}^{(1)} = \frac{\langle \Psi_0 | W_{A,B} | \mathcal{A}\Psi_0 \rangle}{\langle \Psi_0 | \mathcal{A}\Psi_0 \rangle}, \tag{1.12}$$

where $\mathcal{A}$ is the full antisymmetrizer. Equation 1.12 now includes the effect of electron exchange (to all orders) in the first-order energy and is called the Heitler-London energy. At first order, the exchange interaction between two molecules is positive and has been shown to be dependent on the strength of the orbital overlap between the two charge distributions.[8, 9]

Higher-order perturbations using equation 1.3 provide the correct asymptotic expansion, but neglecting the Pauli principle results in a divergent series for short-range interactions.[2, 10] The symmetry-adapted perturbation theory (SAPT) method from Szalewicz and coworkers[11] has been introduced to correct this problem. We have identified that properly accounting for exchange interactions for higher-order perturbations can greatly improve model potential accuracy.[12] Also, since the SAPT procedure does not perform a multipolar expansion of the interacting molecules, short–range penetration interactions arising from charge penetration are properly treated.[13]

While the discussion above considered only two interacting molecules, significant progress has been made in understanding the non-additive many–body interactions that result for 3 or more interacting species.[11, 14, 15, 16, 17, 18]

Although several *ab initio* packages exist to calculate intermolecular interaction energies, in order to study very large systems, model potentials must be developed. Such potentials are generally developed to accurately reproduce *ab initio* energies for small molecules or clusters. These model potentials are typically based on the multipolar expansions of the energy contributions introduced above. With careful choice of the parameters describing the interactions, accurate potentials can be obtained to describe cluster and bulk properties. As will be shown, simple model potentials for water clusters can be created which can quantitatively predict intermolecular and excess electron binding energies.

2.0 THE DISTRIBUTED POINT POLARIZABLE WATER MODEL

This work has been published as Ref. [19]

2.1 INTRODUCTION

It is now widely appreciated that if a water model is to successfully describe water in environments as diverse as clusters, interfaces, and the bulk, explicit inclusion of polarization is essential.[20, 21, 22, 23, 24] In recent work from our group, it has become clear that even water models that explicitly include polarization can encounter difficulties in properly describing the relative energies of various isomers of water clusters.[25] This has motivated us to examine in detail three popular polarizable water models, the Dang-Chang[26] (DC), TTM2-R[27], and AMOEBA[28] models. Three specific issues are addressed: (1) the sensitivity of the interaction energies on the representation of the charge distribution of the monomer, (2) the relative performance of models that employ three, as opposed to one polarizable site, and (3) the importance of including repulsion interactions between all atoms of different monomers rather than just between the O atoms. In exploring these issues, each model is applied to the water dimer, selected isomers of the $(H_2O)_6$ and $(H_2O)_{21}$ clusters, and to several structures of $(H_2O)_7$ that correspond to local minima on the $(H_2O)_7^-$ potential energy surface. The performance of the various models is judged by comparison with the results of *ab initio* MP2 electronic structure calculations. The three water models singled out for study are well suited for addressing these issues since the DC model employs three point charges to represent the charge distribution of the monomer and a single polarizable site, the TTM2-R model employs three point charges and three polarizable sites, and the

AMOEBA model uses a distributed multipole representation of the charge distribution and three polarizable sites. The three models also differ in terms of how they treat dispersion and short-range repulsion interactions between monomers.

Guided by the analyses of the performance of the DC, TTM2-R and AMOEBA models on the test systems, we introduce a new distributed point polarizable (DPP) model, with three permanent charges to represent the static charge distributions of the monomers, and three mutually interacting polarizable sites. The DPP model includes dispersion interactions between the oxygen atoms and repulsion interactions between all atoms of different monomers. The DPP model gives 3–body interaction energies in closer agreement with MP2 results for all water clusters examined and is also found to be quite successful at predicting relative energies. The DPP model is also tested in molecular dynamics simulations of bulk water, for which it is found to give radial distributions functions and other properties in good agreement with experiment.

2.2 THEORETICAL METHODS

The key characteristics of the DC, TTM2-R, AMOEBA, and DPP water models are summarized in Table 1, and the permanent moments and polarizabilities of the water monomer, as described by each of the considered water models, are compared with the experimental values in Table 2. The DC and TTM2-R models employ rigid monomers with the OH bond lengths and HOH angles equal to the corresponding experimental values. (Here, the experimental geometry is taken to be that corresponding to the potential energy minimum rather than to the vibrationally averaged structure.) The AMOEBA model allows for distortion of the monomers and employs for the equilibrium geometry of the monomer the experimental value of the OH bond length and an HOH angle of 108.5°, somewhat larger than the experimental value of 104.52°. Although the non-rigid version of the TTM2 model[29] has been used in much of the work from the Xantheas group, for the present study, we find it advantageous to focus on the rigid version of this model. Also, although the AMOEBA model employs flexible monomers, by artificially increasing the force constants, rigid monomer results can

be generated with it as well. Both the DC and TTM2 models employ three point charges, $+q$ on each H atom and $-2q$ on an M site, located on the rotational axis, slightly displaced from the O atom toward the H atoms to represent the charge distribution of the monomer, whereas the AMOEBA model uses distributed multipoles through the quadrupole on each atom to represent the static charge distribution. The charges used in the DC and TTM2-R models result in dipole and quadrupole moments close to the corresponding experimental values of the monomer, whereas the monomer as described by the AMOEBA model has dipole and quadrupole moments slightly smaller than the experimental values. The underestimation of the dipole moment of the water monomer in the AMOEBA model is a consequence of the use of an HOH angle larger than experiment, whereas the underestimation of the quadrupole moment in this model is primarily due to the use of a reduced (by 27%) atomic quadrupole on the O atom. The electrostatic interactions are damped at short distances in the TTM2-R model but not in the DC or AMOEBA models.

The DC model employs a single isotropic point polarizable site located at the M site, whereas the TTM2-R and AMOEBA models each employ three mutually interacting, atom-centered point polarizable sites. In the latter two models, the permanent moment-induced dipole and induced-dipole–induced-dipole interactions are damped according to a procedure introduced by Thole.[30] Both the DC and TTM2-R models include dispersion and short-range repulsion interactions between O atoms only, in the former case by use of a Lennard-Jones potential and in the latter case *via* R^{-12}, R^{-10}, R^{-6} terms. The AMOEBA model, on the other hand, uses buffered R^{-14} plus R^{-7}[31] interactions between all atoms of different monomers to represent short-range repulsion and dispersion, respectively.

Large basis set MP2 calculations are used to provide benchmark results for testing the various model potentials. It should be noted that several studies have shown that the binding energies of water clusters are not appreciably altered by inclusion of correlation effects beyond second order[32, 33]. For the water dimer comparison is made with the results of MP2 calculations with the aug-cc-pV5Z basis set[34] for $(H_2O)_6$, comparison is made with complete-basis set limit MP2 results,[35] and for $(H_2O)_{21}$ and $(H_2O)_7$, comparison is made

Table 1: Comparison of the DC, AMOEBA, TTM2-R, and DPP water models[a]

	Electrostatics
DPP	point-charges[b]
AMOEBA	distributed multipoles[c]
TTM2-R	point-charges[b,d]
DC	point-charges[b]
	Repulsion+Dispersion
DPP	all-atom exponential repulsion and oxygen R^{-6}
AMOEBA	all-atom buffered R^{-14},R^{-7}
TTM2-R	oxygen R^{-6},R^{-10},R^{-12}
DC	oxygen R^{-12},R^{-6}
	Induction
DPP	all-atom induced dipoles
AMOEBA	all-atom induced dipoles
TTM2-R	all-atom induced dipoles
DC	M-site induced dipole

[a]The DC, AMOEBA, and TTM2-R models are described in Refs. [26], [28], and [27], respectively.

[b]The negative charge is located at the M-site located on the rotational axis and displaced 0.215, 0.25, and 0.25 Å toward the H atoms in the DC, TTM2-R, and DPP models, respectively.

[c]The oxygen atom quadrupole moment is reduced by 27%.

[d]The point-charge interactions are damped through an extension of Thole's procedure. (Ref. [30])

with the results of MP2/aug-cc-pVTZ calculations. The MP2 results for $(H_2O)_6$ and $(H_2O)_{21}$ are taken from the work of Xantheas *et al.*[36, 37, 38, 39] and Cui *et al.*[25], respectively.

Comparison of the results from the various potentials with those from the MP2 calculations has led us to introduce a new model that shares some features with the TTM2-R and AMOEBA models. We designate this model as DPP, referring to its use of distributed point polarizable sites. A description of the the DPP model is provided later in this paper.

Although the DPP model was designed primarily for the characterization of water clusters, it is important to establish that it provides a reasonable description of liquid water as well, and for this reason it was also used in NVT and NPT molecular dynamics simulations (MD) of liquid water at $T = 300K$. The simulations employed a periodic cubic box containing 216 water molecules. Integration of the equations of motion was performed through use of the Beeman[40] algorithm with a 1 fs time step, and with long-range electrostatics being calculated using Ewald summation. The monomers were kept rigid by the use of the RATTLE algorithm.[41] The simulations in the NVT ensemble made use of a box of length 18.643 Å and the Nosé-Hoover thermostat. The density (ρ) and average potential energy (U) were determined as arithmetic means from an isothermal-isobaric (NPT) simulation at 300 K and 1 atm. In the latter simulation, coupling to Groningen-style baths with coupling times of 0.1 ps and 2.0 ps was used to maintain temperature and pressure, respectively.[42] Averages were obtained from 100 ps production runs, following 200 ps equilibration periods.

The self-diffusion constant (D) was determined from the Einstein formula

$$D = \frac{1}{6} \lim_{t\to\infty} \frac{d}{dt} \left\langle \left| r(t) - r(t_0) \right|^2 \right\rangle , \tag{2.1}$$

where the ensemble average of the mean-square displacement was found by averaging over different time origins t_0. In practice, the self-diffusion constant was determined from the slope of the mean square displacement calculated over the NPT run.[28] The specific heat (C_v) was calculated from fluctuations of the total energy (E) according to Ref. [43].

$$C_v = \frac{\langle \delta E^2 \rangle}{k_B T^2}. \tag{2.2}$$

The *ab initio* electronic structure and MD calculations carried out in this study were performed using the Gaussian 03[44] and TINKER[45] programs, respectively.

2.3 COMPARISON OF THE DC, TTM2-R AND AMOEBA MODELS FOR THE WATER MONOMER AND DIMER

In this section, we compare for the water monomer the electrostatic potentials from the DC, TTM2-R, and AMOEBA models, and from MP2 calculations. We then examine for each model the electrostatic, induction, dispersion, and short-range repulsion interactions as a function of the distance between the two monomers in the water dimer. In this case we also report the results of symmetry adapted perturbation theory (SAPT)[46, 11, 47] performed using the aug-cc-pVTZ basis set[48].

2.3.1 Electrostatics

In order to assess the performance of the various models for representing the electrostatic potential of the water monomer, we report in Fig. 1 the difference between the electrostatic potential associated with each model and that calculated at the MP2/aug-cc-pVTZ level of theory, using the same geometry as employed by the model potential under consideration. We note that the electrostatic potentials of the water monomer calculated using the MP2/aug-cc-pVQZ[49] and QCISD[50]/aug-cc-pVTZ methods are nearly identical to that calculated using the MP2/aug-cc-pVTZ method, thereby justifying the use of the latter in assessing the electrostatic potentials from the model potentials.

Figure 1 reports, for the various models, the difference contours at the ± 0.5 kcal/mol level, both in the plane and perpendicular to the plane of the monomer. The ± 0.5 kcal/mol contours were chosen for display because they represent a sizeable (10%) portion of the net binding energy of the water dimer. From Figure 1, it is seen that the electrostatic potential differences for DC, TTM2-R and AMOEBA water models are greater than 0.5 kcal/mol when the test charge is brought within 2 Å of the H or O atoms. This is a pertinent distance as it corresponds roughly to the H-bond distance at the equilibrium geometry of the water dimer. Moreover, for each of these models the out-of-plane electrostatic potential difference plots displays two lobes reminiscent of the lone pairs of the O atom.

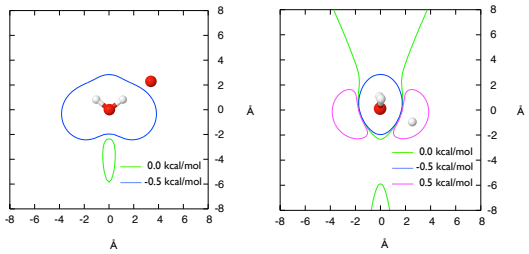

(a) DC: In-plane (b) DC: Out-of-plane

(c) TTM2: In-plane (d) TTM2: Out-of-plane

(e) AMOEBA: In-plane (f) AMOEBA: Out-of-plane

(g) GDMA: In-plane (h) GDMA: Out-of-plane

Figure 1: Model potential − MP2/aug-cc-pVTZ electrostatic potential difference plots. An extra oxygen atom is depicted in the figures showing the in-plane differences, and an extra hydrogen atom is depicted in figures showing the out-of-plane differences in order to indicate the location of the second water molecule in the optimized geometry of the water dimer.

Table 2: Multipole moments and polarizability of the water monomer for various models and from *ab initio* calculations.

		Quadrupole[a](Debye-Å)			Polarizability[a](Å^3)		
	Dipole (Debye)	Q_{xx}	Q_{yy}	Q_{zz}	xx	yy	zz
MP2[b]	1.851	2.62	−2.47	−0.15	1.47	1.37	1.41
QCISD[c]	1.855	2.57	−2.42	−0.14	1.45	1.32	1.37
DC	1.849	2.24	−2.05	−0.19	1.44	1.44	1.44
TTM2	1.853	2.51	−2.23	−0.28	1.61	1.29	1.37
DPP	1.853	2.51	−2.23	−0.28	1.61	1.29	1.37
AMOEBA[d]	1.772	2.40	−2.17	−0.33	1.67	1.23	1.33
	(1.853)	(2.35)	(−2.16)	(−0.20)	(1.66)	(1.22)	(1.33)
GDMA[e]	1.851	2.62	−2.47	−0.15	–	–	–
exp.[f]	1.855	2.62	−2.49	−0.13	1.53	1.42	1.47

[a]In each calculation, the monomer is oriented in the xz plane, with the rotational axis being along the z-axis.
[b]MP2/aug-cc-pVTZ calculations at the experimental geometry.
[c]QCISD/aug-cc-pVTZ calculations at the experimental geometry.
[d]Numbers in parenthesis are for the experimental H-O-H bond angle of 104.52°.
[e]Distributed multipoles determined from MP2/aug-cc-pVTZ calculations.
[f]Dipole: Ref. [51]; Quadrupole: Ref [52]; Polarizability: Ref. [53]

Figures 1(g) and 1(h) report the difference between the electrostatic potential calculated at the MP2/aug-cc-pVTZ level and that calculated using a GDMA representation[54], employing multipoles through the quadrupole on each atom, of the MP2/aug-cc-pVTZ charge distribution. The GDMA method provides a more realistic representation of the electrostatic potential of the water monomer at short distances than do the DC, TTM2-R, or AMOEBA models. In addition, the difference between the GDMA and MP2 electrostatic potentials (at least at the ±0.5 kcal/mol contour level) does not display the "lone-pair-like" lobes found for the corresponding difference potentials for the DC, TTM2-R and AMOEBA models.

Since the AMOEBA model employs a GDMA representation of the MP2 charge density with multipoles through quadrupole on each atom, the discrepancy between its electrostatic potential for the monomer and that from our GDMA fit to the MP2 charge density is surprising. However, there is a straightforward explanation of this discrepancy, namely that it results from the 27% reduction of the oxygen atom quadrupole in the AMOEBA model from the value obtained from the GDMA analysis. This reduction was introduced by Ren and Ponder to improve the geometry of the water dimer as optimized by the AMOEBA model.

Figure 2 displays, for each model considered, the electrostatic interaction energy of the water dimer as a function of the separation between the two monomers (R_{OO}). In generating this plot, the monomers were kept rigid with OH bond lengths and HOH angles appropriate for the experimental gas-phase monomer, and the flap angles that give the orientation of the two monomers with respect to the O–O axis were frozen at the values they have for the MP2/aug-cc-pVTZ optimized structure, *i.e.*, $\theta_{\text{acceptor}} = 58.19°$ and $\theta_{\text{donor}} = 62.6°$, where the angles are defined in Figure 3. For R_{OO} values greater than about 3.5 Å the DC, AMOEBA, and TTM2-R models give nearly the same electrostatic interaction energies for the dimer. However for $R_{OO} = 2.9098$ Å, the O–O distance obtained in the rigid monomer MP2 geometry optimization, the electrostatic interaction energy from the AMOEBA model is about 0.8 kcal/mol more attractive than that from the DC or TTM2-R models. At shorter distances, the TTM2-R model has the weakest electrostatic interaction due to the of damping of the charge-charge interactions. Figure 2 also reports the electrostatic interaction for the water dimer calculated using the GDMA representation of the charge distribution. At R_{OO}

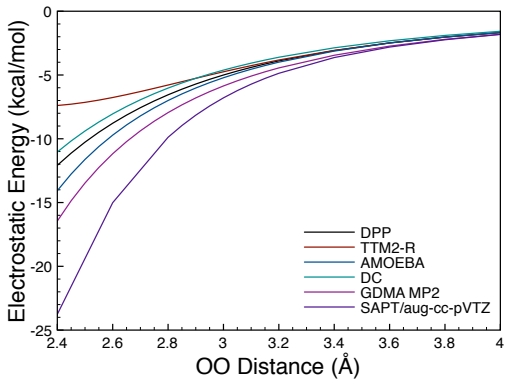

Figure 2: Electrostatic interaction energy for the water dimer, as a function of O–O distance, assuming rigid monomers and fixed flap angles.

= 2.9 Å, the electrostatic interaction calculated using the GDMA procedure is about 0.8 kcal/mol more attractive than that obtained using the AMOEBA model.

The DC, AMOEBA, and GDMA models do not account for changes in the electrostatic interaction resulting from charge penetration effects, which have been reported to lead to an enhancement by about 0.9 kcal/mol in the electrostatic interaction near the equilibrium geometry.[55, 56, 57, 13] At long range ($R_{OO} \geq 3.6$ Å), the electrostatic energy calculated using the GDMA multipoles agree with the SAPT electrostatic potential. At shorter separations, the SAPT potential is more attractive due to charge penetration. As noted above, damping in the TTM2-R model necessarily weakens the electrostatic interactions at short range. For this reason, we believe it is more realistic to employ undamped electrostatics as in the DC and AMOEBA models than damped electrostatics as employed in the TTM2-R model. It is important to note however that the fitting procedure used in developing the TTM2-R water model largely compensates for the underestimation of the electrostatic interactions through a weakening of the short-range repulsion part of the potential as will be seen below.

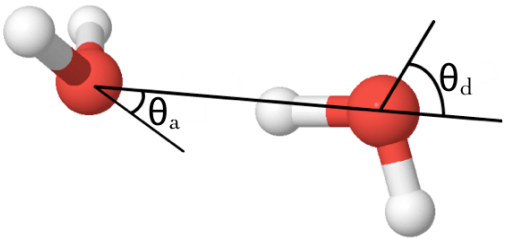

Figure 3: Definition of the angles defining the relative orientation of the monomers in the water dimer.

2.3.2 Induction

Figure 4 displays, as a function of the separation between the monomers, the induction energy of the water dimer calculated with the DC, TTM2-R, and AMOEBA models along with SAPT/aug-cc-pVTZ results (obtained by combining the pure induction and exchange-induction contributions). The curves were calculated using rigid monomers and fixed flap angles as described above. Near the equilibrium geometry of the dimer ($R_{OO} \sim 2.9$ Å), the induction energy calculated using the DC, TTM2-R, and AMOEBA models is -0.77, -0.91 and -1.28 kcal/mol, respectively. The small value of induction energy calculated using the DC model is primarily a consequence of the use of only a single polarizable site on each monomer. The models that distribute the polarizable sites give larger (in magnitude) induction energies primarily because of short, ≈ 2 Å, distances between the H and O atoms forming the hydrogen bond. As $R_{OO} \to 0$, the induction energy from the DC model diverges due to the lack of damping of the interactions involving the induced dipoles. In contrast, in the $R_{OO} \to 0$ limit, the induction energy remains finite in the TTM2-R and AMOEBA models due to the use of a Thole-type damping of the interactions involving the induced moments. For O–O distances less than about 3.2 Å, the induction interaction is appreciably smaller in magnitude in the TTM2-R than in the AMOEBA model. This is primarily a consequence of the use of a stronger damping of the interactions between the permanent and induced moments in the former model. SAPT[46, 11, 47] calculations give induction energies somewhat larger in magnitude than those from the AMOEBA model for $R_{OO} < 3.2$

Å, providing further evidence that the use of distributed polarizable sites is important for describing the short-range induction, and suggesting that the charge-induced dipole interactions in the TTM2-R and AMOEBA models maybe too strongly damped. Several factors likely contribute to the larger magnitudes of the induction energies calculated using the SAPT procedure compared to the model potentials including the inclusion of charge transfer interactions which have been estimated to be about 1 kcal/mol near the minimum,[56] and also contributions from the dipole-quadrupole polarization. We return to this issue in section 2.3.7.

Even though this section has as its focus the role of induction in the interaction between two water monomers, it is instructive to briefly consider the role of 3–body interactions in larger water clusters. If we assume that the 3–body interaction energy is dominated by induction, this then provides a valuable approach for assessing the effectiveness of various water models for describing induction.[17] A detailed analysis of the 3–body energies obtained from the model potentials is presented in section 2.3.7. Here we note that both the DC and TTM2-R models give smaller, while AMOEBA gives larger, (in magnitude) 3–body interaction energies than obtained from MP2 calculations. Although these results appear to support the conclusion reached above that the TTM2-R model underestimates the induction interaction, we should keep in mind that there are contributions to the 3–body energy other than induction.

2.3.3 Repulsion and Dispersion

Figure 5 plots for each of the DC, TTM2-R, and AMOEBA models and SAPT/aug-cc-pVTZ the repulsion, dispersion, and repulsion+dispersion contributions to the energy of the water dimer as a function of OO separation (again for rigid monomers and fixed flap angles). With the DC and TTM-R models, we associate the dispersion interaction with the R^{-6} contributions, and with the AMOEBA model we associate it with the buffered R^{-7} contribution. Similarly for the DC, TTM2-R, and AMOEBA models we associate the exchange-repulsion interactions with the R^{-12}, R^{-10} plus R^{-12}, and buffered R^{-14} contributions, respectively. Because the repulsion and dispersion contributions differ appreciably from model to model,

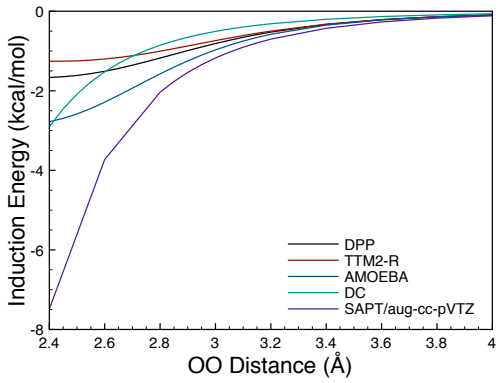

Figure 4: Induction energy of the water dimer as a function of the separation between the monomers, with rigid monomers and fixed flap angles.

it is somewhat more instructive to examine the sum of these two terms.

At $R_{OO} = 2.9$ Å, the repulsion+dispersion contributions from the DC, TTM2-R, and AMOEBA models are 1.3, 1.2, and 2.2 kcal/mol, respectively. However, at $R_{OO} = 2.5$ Å, the repulsion+dispersion contribution from the TTM2-R model is about 7 kcal/mol smaller than that from the DC and AMOEBA models. Because the repulsion+dispersion part of the TTM2-R potential was obtained by fitting to MP2 interaction energies with the electrostatic and induction contributions subtracted out, and because these interactions are underestimated in magnitude in this model, at short distances the resulting repulsion+dispersion interaction is necessarily weaker than that in the DC and AMOEBA models. Over the range $2.6 \leq R_{OO} \leq 3.8$ Å, the dispersion contribution from the SAPT calculations is more attractive than that from any of the model potentials, with the exception of TTM2-R. In part, this is due to the SAPT calculations recovering the higher order (*i.e.* C_7, C_8, *etc.*) dispersion contributions. From Fig. 5(c), it is seen that the SAPT repulsion+dispersion curve is much more repulsive than that from any of the model potentials. To a large extent, this is offsetting the larger (in magnitude) electronic and induction contributions obtained from the SAPT calculations.

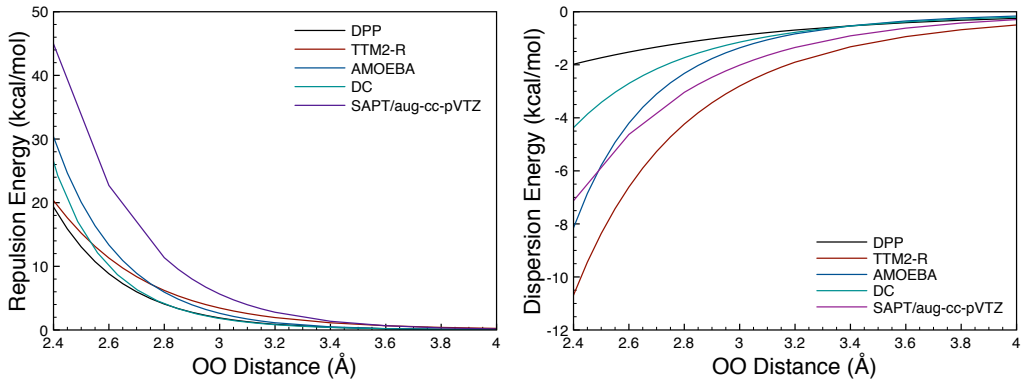

(a) Repulsion energy

(b) Dispersion energy

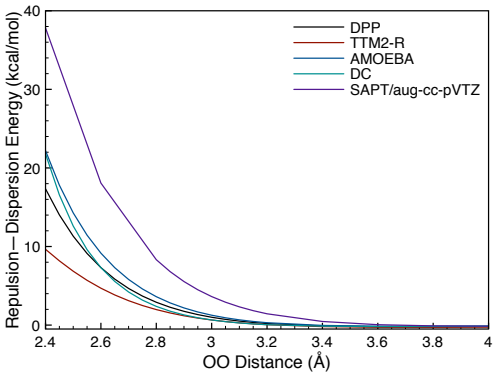

(c) Repulsion + Dispersion energy

Figure 5: Repulsion and dispersion energies for $(H_2O)_2$ as a function of O–O separation, with rigid monomers and fixed flap angles.

2.3.4 Net Interaction Energies

In the previous sections, we examined for the DC, TTM2-R and AMOEBA model potentials how the electrostatic, induction, dispersion, and repulsion interactions for the water dimer vary with the O–O separation, with fixed monomer geometries and fixed flap angles. In Fig. 6(a), the potential energy curves obtained by combining these contributions are plotted. The corresponding MP2/aug-cc-pV5Z potential energy curve is included for comparison. Fig. 6(b) reports the corresponding difference of the energies using the various model potential and the MP2/aug-cc-pV5Z calculations. The MP2/aug-cc-pV5Z calculations give a binding energy of −4.98 kcal/mol, within 0.01 kcal/mol of the MP2/CBS result.[35]

Although the DC model underestimates the magnitude of the binding energy of the dimer by about 0.4 kcal/mol, both the TTM2-R and AMOEBA models give binding energies within 0.1 kcal/mol of the MP2/CBS limit. As seen from Fig. 6(b), potentials calculated using the DC, AMOEBA, and TTM2-R models all rapidly diverge from the MP2 potential for $R_{OO} \lesssim 2.7$ Å, with the TTM2-R potential being more attractive and the DC and AMOEBA potentials more repulsive than the corresponding MP2 potential. Interestingly, all the model potentials are less attractive than the MP2 potential at R_{OO} values between 3 and 4 Å, and for the AMOEBA model this is the case for longer distances as well. The error in the long-range interaction energy as calculated with the AMOEBA model is primarily due to the scaling of the oxygen atom quadrupole moment.

Additional insight into the viability of the various water models is provided by examining the variation of the interaction energy of the dimer with O–O distance, with the angles defining the relative orientation of the two water monomers being optimized at each O–O distance considered (but still keeping the water monomers frozen at the experimental gas-phase geometry of the isolated monomer). The variations of the two flap angles with O–O separation are reported in Fig. 7, and the associated potential energy curves are shown in Fig. 8(a). For all theoretical methods considered, the flap angles undergo a rapid change near $R_{OO} = 2.55$ Å. The changes in the flap angles are more abrupt in the MP2 calculations than for any of the model potentials, with the best agreement with the MP2 results being for the AMOEBA model, and significantly poorer agreement being found with the DC and

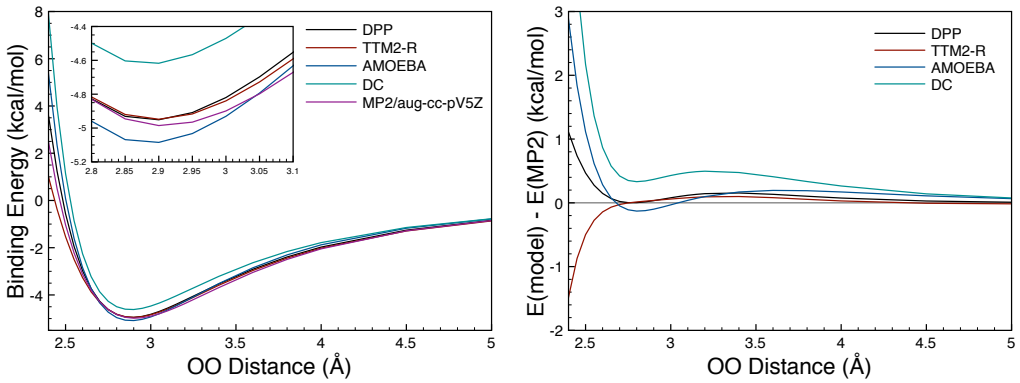

(a) Total energies

(b) Total energy differences from MP2

Figure 6: (a) Potential energy curves for the water dimer calculated with fixed flap angles; (b) differences between the total energies from various models and the MP2 energies

TTM2-R models. As seen in Fig. 8(a), although the MP2 and AMOEBA potential energy curves with relaxed flap angles vary smoothly near $R_{OO} = 2.55$ Å, the corresponding DC and TTM2-R potentials have kinks near this separation between the monomers. When the flap angles are relaxed, the TTM2-R potential becomes too repulsive at short R_{OO} ($R_{OO} \lesssim 2.6$ Å) values, in contrast to the situation found for fixed flap angles (compare Figures 6(b) and 8(b)).

Fig. 9 displays, as a function of R_{OO}, the repulsion+dispersion and the electrostatic+induction interaction energies for each of the three model potentials using flap angles optimized at the MP2/aug-cc-pVTZ level at each O–O distance. For all three models there is a kink in the electrostatic+induction contribution to the energy for $R_{OO} \sim 2.55$ Å. However, in the case of the AMOEBA model this kink is approximately cancelled by a kink in the opposite direction in the repulsion potential. In contrast, the repulsion potentials for the DC and TTM2-R models vary smoothly with R_{OO}, and thus cannot cancel the kink from the electrostatic interactions. The absence of the countering kink in the repulsive potential of these two models is a consequence of their employing repulsion interactions between O atoms only.

These results indicate that it is necessary to include repulsion interactions between all atoms of the two monomers in order to properly describe the potential energy surface of the

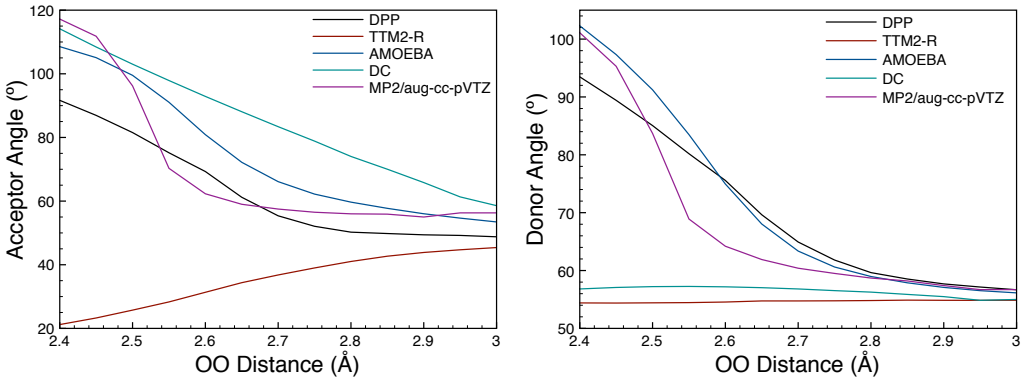

(a) Dimer acceptor angle (θ_a) (b) Dimer donor angle (θ_d)

Figure 7: Variation of the flap angles of the water dimer as a function of the O–O separation.

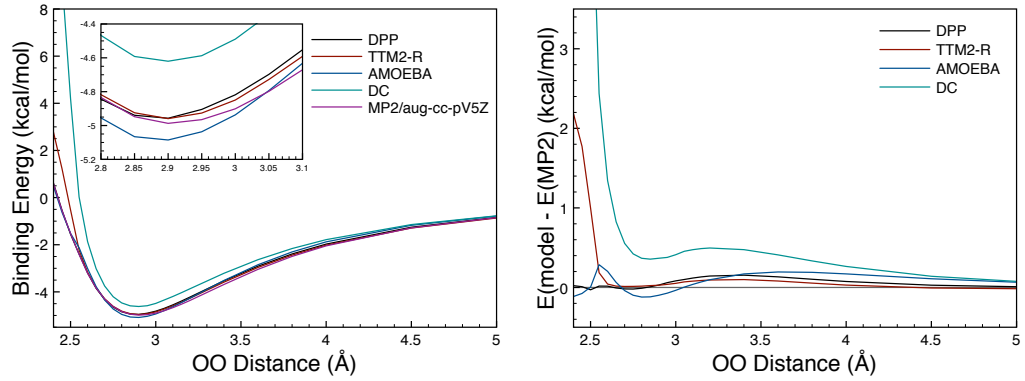

(a) Total energies (b) Total energy differences from MP2

Figure 8: (a) Potential energy curves of the water dimer with relaxed flap angles; (b) the associated differences between the total energies from various models and the MP2 energies. All results are for MP2/aug-cc-pVTZ optimized geometries, with flap angles being optimized at each O–O distance.

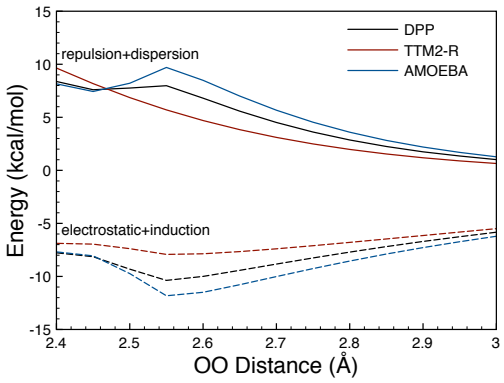

Figure 9: Repulsion+dispersion and electrostatics+induction interaction energies of the water dimer as a function of O–O distance, with flap angles optimized at the MP2/aug-cc-pVTZ level.

water dimer for O–O distances less than about 2.65 Å. This is an important observation as many other popular water models share with the DC and TTM2-R models the use of repulsion interactions between O atoms only and because O–O distances as short as 2.65 Å occur in the equilibrium structures of the larger clusters.

2.3.5 The DPP water model

Extensive calculations on a large number of water clusters using several water models in addition to the DC, TTM2-R, and AMOEBA models, has led us to conclude that for describing water clusters it is more important to employ three mutually interacting polarizable sites and to include repulsion interactions between all atoms than it is to adopt a more sophisticated representation of the charge distribution than that provided by three point charges. Evidence in support of this conclusion will be provided in the following section where we examine selected isomers of $(H_2O)_6$, $(H_2O)_7$, and $(H_2O)_{21}$. This has led us to introduce a new water model which, like the TTM2-R and AMOEBA models, employs three atom-centered polarizable sites. The key features of the distributed point polarizable (DPP) model are:

(1) The permanent charge distribution of the monomer is described using the three point

charges of the TTM2-R model. However, the charge–charge interactions between monomers are not damped.

(2) The model employs three mutually interacting polarizable sites with Thole–type damping.[30] The atomic polarizabilities are the same as those employed in the TTM2-R and AMOEBA models, *i.e.*, 0.496 and 0.837 Å^3 for H and O, respectively. The exponent damping the permanent moment (charge)–induced dipole interactions is chosen to be 0.23, which is slightly less strongly damped than TTM2-R (0.2), but not as weak as AMOEBA (0.39). The charge-dipole damping parameter in the DPP model was chosen so that the relative binding energies for selected isomers of the water hexamer are close to the MP2 results. The exponent in the factor damping the induced dipole–induced dipole interactions is 0.3, 0.39, 0.3, with the TTM2-R, AMOEBA, and DPP models, respectively. The DPP induction energy for the water dimer as a function of O–O separation has been plotted in Figure 4, from which it is seen that for O–O distances less than about 3.4 Å, the induction energy obtained from the DPP model is intermediate between that calculated with the TTM2-R and AMOEBA models.

(3) Dispersion interactions are included *via* damped R^{-6} terms between O atoms only, with the damping function,

$$f(\delta, R) = 1 - e^{-\delta R} \left(\sum_{k=0}^{6} \frac{(\delta R)^k}{k!} \right), \tag{2.3}$$

being taken from Tang and Toennies.[58] The parameters C_6 and δ were chosen to be 1300 Å^{6}kcal/mol and 2.23 Å^{-1}, respectively. This C_6 value is about 30% greater than the known value of C_6. The use of an enhanced C_6 can be viewed as a crude way of incorporating C_8 and C_{10} contributions to the interaction energy for geometries near the potential minimum. With this choice of C_6 and δ, the dispersion contribution is -1.0 kcal/mol, at $R_{\mathrm{OO}} = 2.9$ Å.

(4) Exponential repulsion interactions are included between all atoms of different monomers. The six parameters in the repulsion terms of the DPP model were determined using MP2/aug-cc-pV5Z energies for the one dimensional potential for the water dimer calculated using relaxed flap angles. Specifically, at each structure for $2.4 \leq R_{\mathrm{OO}} \leq 3.1$ Å, the electrostatic, induction, and dispersion contributions of the DPP model were subtracted from the corresponding MP2/aug-cc-pV5Z energies, to give an estimated repulsion potential to which the

repulsion part of the DPP potential was fit. The parameters are shown in Table 3. For the case that the flap angles are optimized at each value of the O–O separation in Fig. 6, the dimer potential calculated with the DPP model is free of the kink found in the DC and TTM2-R models.

2.3.6 Comparison of various water models for stationary points on the dimer PES

As a further test of the DC, TTM2-R, AMOEBA, and DPP water models, we consider the ten stationary points on the water dimer potential energy surface characterized by Smith *et al.*[59] This includes the global minimum, three first-order saddle points, and six higher-order saddle points.[33] In order to facilitate comparison of the model potential and MP2 results, we re-optimized all stationary points at the MP2/aug-cc-pVTZ level of theory, assuming rigid monomers. These were followed by single-point MP2/aug-cc-pV5Z and model potential calculations using these geometries.

The results of these calculations are summarized in Figure 10, from which it is seen that the largest discrepancies between the model potential and MP2 results occur for structures 4-7. Three of these structures are "cyclic" the fourth is a H-bonding dimer with $\theta_{\rm d} = 117.7^\circ$ and $\theta_{\rm a} = 138.1^\circ$. All models considered under-bind these four structures with the under-binding being greatest with the DC model and the smallest with the DPP model. The root mean square (rms) deviation of the binding energies with the AMOEBA and DPP models are 0.45 and 0.24 kcal/mol, respectively. With the TTM2-R model, these four stationary points are predicted to be $0.8 - 1.1$ kcal/mol less strongly bound than at the MP2/aug-cc-pV5Z level. Overall, the DPP model reproduces the energies of the test set significantly better than the TTM2-R and AMOEBA models.

Table 3: Key parameters of the DPP model.

Site	charges	polarizability (Å^3)		
H	0.5742	0.496		
O		0.837		
M	−1.1484[a]			
O-M (Å)	0.250			
Interaction		repulsion[b]	dispersion[c]	
	A	b	C_6	δ
O–O	1.15272∗10^5	4.1679	−1300.	2.23
O–H	1.80366∗10^3	3.5355		
H–H	1.19085∗10^5	5.5817		
Damping parameters for induction				
charge–induced dipole	0.23			
induced dipole–induced dipole	0.3			

[a] A polarizability of 0.837 Å^3 is used for the M-site in the function damping the charge–induced dipole and induced dipole–induced dipole interactions.

[b] The first parameter is the pre-exponential factor, A (kcal/mol), and the second is the coefficient, b (1/Å) in the equation $Ae^{(-br)}$.

[c] The first parameter is the dispersion coefficient, C_6 (Å^6 kcal/mol), and the second is the damping parameter, δ (1/Å).

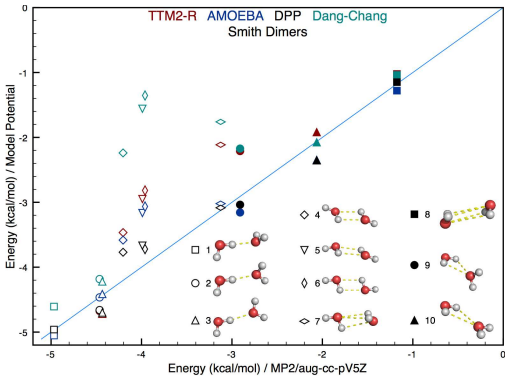

Figure 10: Interaction energies for the ten stationary points on the potential energy surface of $(H_2O)_2$, calculated using the various model potentials and at the MP2/aug-cc-pV5Z level of theory.

2.3.7 Application of the DPP, TTM2-R, and AMOEBA water models to the $(H_2O)_6$, $(H_2O)_7$, and $(H_2O)_{21}$ clusters

Table 4 summarizes the binding energies, calculated using various theoretical methods, of the lowest energy cage, prism, ring, and book isomers of $(H_2O)_6$. Compared to the complete-basis-set limit MP2 results of Xantheas *et al.*[35], the DC model considerably under-binds (by $4.8 - 5.5$ kcal/mol) these clusters while the AMOEBA, TTM2-R and DPP models all give absolute binding energies in good agreement with the MP2/CBS values, with the rms deviations being 0.10, 0.54 and 0.35 kcal/mol respectively. Moreover, all four models predict the cage, prism, ring, and book isomers of $(H_2O)_6$ to be within 1.6 kcal/mol of one another, with the cage and prism isomers being separated by 0.5 kcal/mol or less. Again it is seen that R^{-12}, R^{-10}, R^{-6} "repulsion-dispersion" term in the TTM2-R model effectively compensates for weaker induction and electrostatics in this model (compared to the AMOEBA and DPP models), at least for the low energy minima on the PES. In the case of the AMOEBA model, binding energies of the various isomers of $(H_2O)_6$ are reduced (in magnitude) by $1.0 - 1.5$ kcal/mol when the monomers are held rigid. Thus it is seen that both the DPP and TTM2-R models, while employing rigid monomers, give interaction energies closer to those expected

Table 4: Water hexamer binding energies and 3–body interaction energies (kcal/mol)

Isomer[a]	MP2/CBS[b]		DC		AMOEBA[c]		AMOEBA-R[d]		TTM2-R		DPP	
Total Interaction Energy												
book	−45.61	(0.25)	−40.43	(0.57)	−45.77	(0.12)	−44.58	(0.32)	−45.10	(0.55)	−45.12	(0.90)
cage	−45.79	(0.07)	−40.86	(0.14)	−45.88	(0.01)	−44.90	(0.00)	−45.65	(0.00)	−45.95	(0.07)
prism	−45.86	(0.00)	−41.00	(0.00)	−45.89	(0.00)	−44.54	(0.36)	−45.11	(0.54)	−46.02	(0.00)
ring	−44.86	(1.00)	−39.39	(1.61)	−44.81	(1.08)	−43.52	(1.38)	−44.30	(1.35)	−44.43	(1.59)
3–body[e]												
book	−7.81	(1.40)	−6.25	(0.80)	−9.96	(0.99)	−9.28	(0.82)	−7.48	(0.82)	−7.94	(1.05)
cage	−6.87	(2.34)	−5.12	(1.93)	−9.07	(1.88)	−8.49	(2.46)	−6.76	(1.54)	−7.09	(1.90)
prism	−6.83	(2.38)	−5.55	(1.50)	−8.55	(2.40)	−7.83	(3.12)	−6.20	(2.10)	−6.72	(2.27)
ring	−9.21	(0.00)	−7.05	(0.00)	−10.95	(0.00)	−10.13	(0.00)	−8.30	(0.00)	−8.99	(0.00)

[a]Geometries have been optimized for each theoretical method considered. Relative energies are in parentheses.

[b]From Ref. [35]

[c]From Ref. [28]

[d]Results obtained using the AMOEBA model but with the monomers held rigid

[e]MP2 3–body results were calculated with MP2/aug-cc-pVTZ at rigid monomer optimized MP2/aug-cc-pVDZ geometries

for a relaxed than for a rigid model.

Table 4 also reports the 3–body contributions to the interaction energy for each approach. From the table it is seen that the AMOEBA model overestimates the 3–body interaction energies in magnitude, differing from the MP2 values by as much as 2.2 kcal/mol. In contrast, the TTM2-R model underestimates (by up to 0.9 kcal/mol) the 3–body interaction energies, while the DPP model gives binding energies nearly identical to the MP2 results.

We consider next the application of the various water models to the five structures of $(H_2O)_7$, depicted in Fig. 11. These isomers correspond to local minima of $(H_2O)_7^-$, located in simulations of the anion[60] and have H-bonding arrangements quite different from those normally found for neutral water clusters. The geometries of the anions were optimized using the MP2 method with a flexible basis set and using rigid monomers.[61] These geometries were then used for single-point MP2/aug-cc-pVTZ and various model potential calculations on the neutral clusters.

Although the considered structures of $(H_2O)_7$ lie high in energy compared to the global minimum of the neutral cluster, they are important in the simulations of the $(H_2O)_7^-$ cluster.

In particular, in model Hamiltonian approaches[62] in which the energy of the anion is given by $E_{\rm neutral}$ + EBE, where $E_{\rm neutral}$ is the energy of the neutral cluster as described by a standard water model and EBE is the binding energy of the excess electron, errors in the relative energies of the neutral clusters translate into errors in the relative energies of the different isomers of the anion. In spite of the successes of the DC, TTM2-R, and AMOEBA models for describing the low-lying potential energy minima of $(H_2O)_n$ clusters, the results presented in Table 5 show that these models are not as successful at predicting the relative energies of structures with H-bonding arrangements appreciably different from those normally encountered in the neutral clusters. Of the models tested, the DPP model is the most successful at reproducing the relative energies of the various $(H_2O)_7$ isomers. The success of the DPP model on this set is a consequence of its providing an accurate description of the 3–body energies and of its inclusion of repulsion interactions between all atoms.[60, 63]

The three–body energies for the five $(H_2O)_7$ clusters are also summarized in Table 5, from which it is seen that the DC model significantly underestimates in magnitude, the 3–body interaction energies, with the errors in the relative 3–body contributions being as large as 1.6 kcal/mol. In contrast, the TTM2-R model slightly underestimates the magnitude of the 3–body interaction energies, while the AMOEBA model overestimates the magnitude of the 3–body interaction energies. Again, DPP is found to give the best description of the 3–body energies with a rms deviation from the MP2 results being only 0.08 kcal/mol.

We examine next the 2– and 3–body interaction energies of the two isomers of $(H_2O)_{21}$. As noted by Cui *et al.*,[25] the relative stability of these two isomers is especially sensitive to the theoretical model employed. Although CBS-limit MP2 binding energies are not available for $(H_2O)_{21}$ we estimate, based on results by Fanourgakis *et al.* for $(H_2O)_{20}$[64], that the CBS-limit binding energies are $6-9$ kcal/mol smaller in magnitude than the MP2/aug-cc-pVTZ results listed in Table 6, with most of the change in the binding energies in going from the aug-cc-pVTZ basis set to the CBS limit being due to the 2–body contributions.

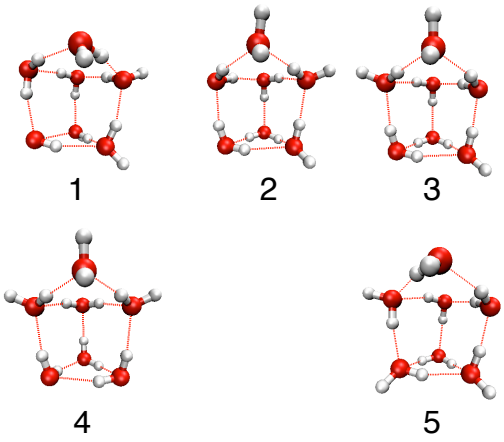

Figure 11: Minimum energy structures of $(H_2O)_7^-$ from ref. [61]

Table 5: Total and 3–body interaction energies of $(H_2O)_7$ at minimum energies structures of $(H_2O)_7^-$

Isomer[a]	MP2/aug-cc-pVTZ[b]		DC		AMOEBA		TTM2-R		DPP	
Total Interaction Energy										
1	−53.30	(0.09)	−45.82	(0.50)	−51.66	(0.54)	−51.94	(0.44)	−52.91	(0.60)
2	−45.42	(7.97)	−40.89	(5.43)	−43.74	(8.46)	−45.29	(7.09)	−45.50	(8.01)
3	−48.41	(4.98)	−43.35	(2.97)	−46.73	(5.47)	−47.98	(4.40)	−48.31	(5.20)
4	−42.98	(10.41)	−39.22	(7.10)	−40.94	(11.26)	−43.43	(8.95)	−42.97	(10.54)
5	−53.39	(0.00)	−46.32	(0.00)	−52.20	(0.00)	−52.38	(0.00)	−53.51	(0.00)
3–body										
1	−6.71	(0.60)	−4.95	(0.66)	−7.92	(0.68)	−6.18	(0.54)	−6.81	(0.59)
2	−3.37	(3.94)	−2.52	(3.09)	−3.77	(4.83)	−2.97	(3.75)	−3.32	(4.08)
3	−4.47	(2.84)	−3.46	(2.15)	−5.01	(3.59)	−3.96	(2.76)	−4.40	(3.00)
4	−1.53	(5.87)	−1.28	(4.33)	−1.60	(7.00)	−1.41	(5.31)	−1.59	(5.81)
5	−7.31	(0.00)	−5.61	(0.00)	−8.60	(0.00)	−6.72	(0.00)	−7.40	(0.00)

[a]The geometries were optimized for the $(H_2O)_7$ anions using the MP2 method with rigid monomer constraints.[61]

[b]MP2 energies of the neutral clusters at the anion geometries.[61]

We consider first the two–body energies for the case of rigid monomers. Whereas the AMOEBA model underestimates (in magnitude) the net rigid-monomer 2–body interaction energy by almost 5 kcal/mol, the TTM2-R and DPP models overestimate the net 2–body energies, giving results closer to the relaxed monomer RIMP2 results. In arriving at these estimates, we have accounted for the extrapolation of the RIMP2 results to the CBS limit.

We now turn to the 3–body interaction energies, again focusing on the rigid monomer results. From Table 6 it is seen that the AMOEBA model overestimates (in magnitude) the net 3–body interaction energies by about 4 kcal/mol and that the TTM2-R and DPP models underestimate the net 3–body energies by about 5 and 3 kcal/mol, respectively. Again, the DPP model fares the best at reproducing the 3–body energies from the rigid monomer MP2 calculations.

2.3.8 Simulations of bulk water

The average density, potential energy, diffusion constant, and heat capacity of liquid water calculated using the DPP, TTM2-R, AMOEBA, and SWM4-NDP[22] force fields, together with the corresponding experimental values, are summarized in Table 7. The densities calculated with the DPP and TTM2-R models are about 8 and 4% higher, respectively, whereas the AMOEBA model gives a density essential identical with the experimental value. The self diffusion constant, calculated using the DPP model, is about 30% larger than the experimental value, consistent with a H-bonding network which is under-structured. The average potential energy, calculated using the DPP model, is about 1.1 kcal/mol greater than the experimental value. However, it has been estimated that quantum corrections are expected to reduce the average energy (U) by ~ 1 kcal/mol which would bring the calculated U for the DPP model into close agreement with experiment. The constant volume heat capacity, calculated using the DPP model, of 19.4 cal mol^{-1} K^{-1} is in good agreement with experiment. Figures 12-14 show the radial distribution functions obtained from the MD simulations using DPP method with the NVT ensemble. The height of the first peak in the O–O radial distribution function, $g_{\mathrm{OO}}(r)$, calculated using the DPP model, is in good

Table 6: 1–, 2– and 3–body interaction energies (kcal/mol) of two isomers of $(H_2O)_{21}$.

hline	TIP4P-gm(21)			DD(20,1)		
Method	1–body	2–body	3–body	1–body	2–body	3–body
RIMP2 (flexible)[a]	10.87	−189.68	−47.21	12.95	−189.16	−51.07
RIMP2 (rigid)[b]	–	−177.83	−39.31	–	−176.00	−41.47
AMOEBA (flexible)[c]	5.90	−173.25	−46.34	6.26	−172.74	−48.63
AMOEBA (rigid)[c]	–	−164.02	−43.48	–	−163.01	−45.69
TTM2-F[c]	4.12	−191.84	−36.66	4.39	−190.88	−37.38
TTM2-R[c]	–	−185.57	−34.92	–	−184.13	−35.53
Dang-Chang[c]	–	−164.08	−35.94	–	−161.05	−36.66
DPP[c]	–	−179.84	−36.34	–	−179.42	−38.48

[a]Single-point RIMP/aug-cc-pVTZ energies at RIMP2/aug-cc-pVDZ optimized geometries.

[b]RIMP2/aug-cc-pVTZ energies with RIMP2/aug-cc-pVDZ geometries, adjusted to restore the monomers to experimental gas-phase geometry.

[c]For each model potential, the geometries have been optimized using that model potential.

Table 7: Properties of liquid water at 298 K.

Method	ρ (g/cm^3)	U (kcal/mol)	D (10^5 cm^2/s)	C_v (cal/(mol K))
SWM4-NDP[a] [b]	1.000	−9.923	2.33	
TTM2-R[c]	1.046	−11.21	2.23	
AMOEBA[d]	1.0004	−9.00	2.02	28.4[e] (20.9)[f]
DPP[g]	1.105	−10.90	2.63	19.0
Experiment[h]	0.9965	−9.91	2.3	17.8

[a] Calculations performed at 298K
[b] Ref. [22]
[c] Ref. [27]
[d] Ref. [28]
[e] Flexible model
[f] Rigid model
[g] This work
[h] ρ and U from Ref. [66], D from Ref. [67], and C_v from Ref. [68]

agreement with the neutron scattering experiments of Soper[65]. However, the second peak from the calculation is weaker and broader than than that determined experimentally, again consistent with an under-structuring. On the other hand, the DPP model overestimates the height of the first peak in both $g_{OH}(r)$ and $g_{HH}(r)$, with the peaks also shifted slightly to the right of the experimental values. Similar trends have previously been observed in simulations with the AMOEBA[28] and other models and are due in part to the neglect of quantum corrections.

2.4 CONCLUSIONS

In this paper we have analyzed the performance of the DC, TTM2-R, AMOEBA, and DPP polarizable water models for selected $(H_2O)_n$ clusters. The DPP model shares several key

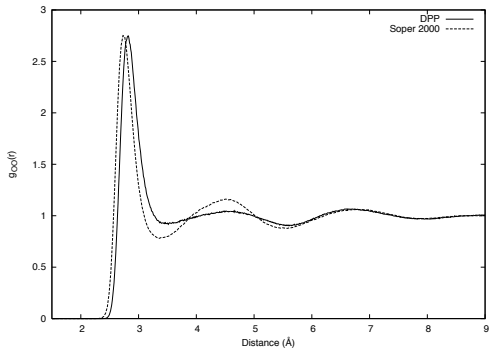

Figure 12: Experimental[69, 65] and calculated O–O radial distribution function.

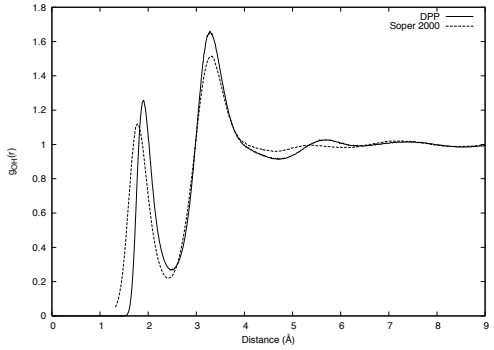

Figure 13: Experimental[65] and calculated O–H radial distribution function.

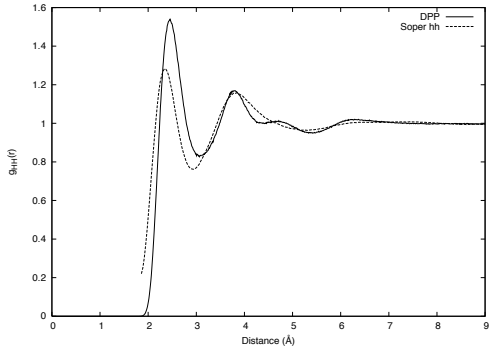

Figure 14: Experimental[65] and calculated H–H radial distribution function.

features with the TTM2-R and AMOEBA models. Specifically, it employs three mutually interacting polarizable sites, but with the charge–induced dipole interactions damped less strongly than in the TTM2-R model. In addition, the DPP model includes repulsion interactions between all atoms (similar to the AMOEBA model, but in contrast with the TTM2-R model which includes repulsion interactions between O atoms only). It is found that explicit inclusion of O–H and H–H repulsion interactions in addition to O–O repulsion is essential for describing the potential energy surface of the water dimer at short O–O distances as well as for describing clusters with "unusual" H-bonding arrangements. By comparison with the results of MP2 calculations it is shown that both the DC and TTM2-R models underestimate in magnitude the 3–body interaction energies in $(H_2O)_n$ clusters, while the AMOEBA model overestimates these energies. The underestimation of the 3–body interaction by the DC model is primarily a consequence of its use of a single polarizable site, whereas the underestimation of the 3–body interaction in the TTM2-R model is due to the choice of the parameters involved in the damping interaction involving induced dipoles. Of the model considered, the DPP model provides the best description of the 3–body interaction energies as judged by comparison to rigid-monomer MP2 results. As noticed previously by Pedulla *et al.*, relaxation of the monomers tends to enhance the 3–body interaction energies.[70]

The only many–body interactions included explicitly in the four water models considered in this work are those due to induction. In fact, analyses of the 3–body interaction energy of $(H_2O)_3$ using the SAPT procedure[17] reveals that 3–body exchange interactions are sizable and typically of the same sign as the 3–body induction terms.[46, 17] As a result, polarizable water models that give for water clusters 3–body energies close to the MP2 values can be viewed as incorporating exchange effects in an effective manner through enhanced induction, much in the same way that the TIP4P[71] and SPC/E[72] account models for polarization effects by use of enhanced charges and dipole moments. Thus, although we have noted that the TTM2-R model tends to give 3–body energies that are smaller in magnitude than the corresponding MP2 results, it probably comes closest of the models considered at representing the 3–body induction interactions. The Szalewicz group has developed, based on their SAPT calculations, a functional representation for 3–body exchange interactions in water[17] and have added this to their 2–body plus induction model in carrying out

simulations of bulk water.[73, 18] The present study suggests that it may be possible to capture the most important contributions due to 3–body exchange by damping out less strongly the short range induction interactions. It remains to be established how effective this approach will be for accurately characterizing water in a range of environments.

3.0 THE DRUDE MODEL FOR INTERACTION EXCESS ELECTRONS WITH WATER CLUSTERS

Manuscript in preparation Thomas Sommerfeld, Albert DeFusco and Kenneth D. Jordan

3.1 INTRODUCTION

Reactions involving electrons in aqueous media are of fundamental importance in a wide range of biological and chemical processes.[74] For example, the passage of radiation through water, ionizes the water, producing free electrons that can subsequently cause electronic excitation or bond cleavage of solute molecules. In addition, electrochemistry in aqueous media necessarily involves electron transfer through water, and electron transfer in photosynthetic reaction centers not only occurs in the presence of water but also explicitly involves water in the redox chemistry.[75]

Although solvated electrons in ammonia have been known since the studies of Weyl in 1864,[76] the hydrated electron (e^-_{aq}), was not identified until the experiments of Hart and Boag in 1962.[77] The hydrated electron has been the subject of numerous experimental and theoretical studies, with much of the emphasis having been placed on elucidating its dynamics following photoexcitation.[78, 79, 80, 81, 82, 83, 84, 85, 86] The ground electronic state of the hydrated electron is generally viewed as consisting of an electron in a approximately spherical cavity of radius ~ 2.2 Å, with the electron binding energy (i.e., the energy required to promote the electron to the conduction band) being 3.2 eV.[78, 87, 88] However, the molecular level structure and the dynamics of the hydrated electron remain a subject of debate.[89] Indeed, it has even been suggested that the hydrated electron is actually due to

a solvated H_3O species.[90]

Recently considerable attention has been focused on $(H_2O)_n^-$ clusters which can be studied by experimental techniques and high-level *ab initio* electronic structure methods that would not be applicable to e_{aq}^-.[91, 92, 93, 94, 95, 96, 97, 98, 61, 99, 100, 101, 102, 103] The combination of theory and experiment on the small $(H_2O)_n^-$ clusters has greatly advanced our understanding of how an excess electron impacts and is accommodated by the H-bonding arrangements. Although the water monomer itself does not bind an excess electron to form a stable anion and does not have low-lying temporary anion states (resonances), the dimer and larger clusters do bind excess electrons.[97, 98, 61, 99, 100, 101, 102, 103, 104, 105, 106, 107] The excess electron in the cluster anions occupies a non-valence orbital, and the stability of the resulting ions derive from the interaction of the excess electron with the static charge distribution of the cluster as well as from induction and dispersion interactions between the excess electron and the electrons of the monomers. While the basic structural motifs of the experimentally observed anions of the $n \leq 7$ clusters are now well established,[96, 97, 98, 61, 99] the structures of the larger clusters remain unknown. In particular, there has been an ongoing debate about the surfaces *vs.* interior nature of the $n \geq 30$ clusters.[101, 102, 103, 104, 105]

Ab initio electronic structure methods have proven extremely valuable in elucidating the role of electron correlation effects on the binding of excess electrons to water clusters.[93, 94, 95, 96, 108, 109] Large basis set CCSD(T)[110] calculations of the electron binding energies (EBE) have been carried out for clusters as large as $(H_2O)_6^-$,[111] and Herbert and Head-Gordon have reported MP2 calculations on selected isomers of $(H_2O)_n^-$ clusters with n as large as 24,[93, 94] with this work recently being extended to clusters as large as $(H_2O)_{33}^-$ by Williams and Herbert.[95] However, comparison with experiment requires inclusion of finite temperature effects through Monte Carlo or molecular dynamics (MD) simulations, sampling 10^7 or more configurations, making *ab initio* (e.g., MP2 or CCSD(T)) methods computationally prohibitive even for clusters as small as the hexamer. Simulations of negatively charged water clusters containing a few tens of monomers are feasible with density functional methods, but the reliability of such simulations would be questionable since commonly used functionals do not properly describe long-range correlation effects,[112] which

can be very important for the binding of excess electrons to water clusters,[108, 109] and they also have problems describing charge localization.[113] In light of these considerations, it is not surprising that most of the theoretical work on moderate to large $(H_2O)_n^-$ clusters as well as of excess electrons in bulk water and in water films has employed model potentials.[83, 84, 85, 86, 114, 115, 116, 117, 118] In the model potential approaches, the total energy of the anion is given by the energy of the neutral water system, as described by a classical force field, plus the binding energy of the excess electron, calculated using a one-electron model Hamiltonian. Although some of the early theoretical work using such model potentials did not allow explicitly for the polarization of the water molecules by the excess electron, it is now recognized that inclusion of electron-water polarization is important for reliable characterization of excess electrons in aqueous media.[117] In general, electronic polarization has been incorporated into the model Hamiltonians by means of damped or cut-off $\alpha/2r_i^4$ terms, where α is the polarizability of a monomer and r_i is the distance from the electron and the polarizable site associated with monomer i. The successes of such models for describing the interaction of excess electrons with aggregates of water is surprising in light of the large body of theoretical work on small water clusters demonstrating that dispersion-type correlation interactions between the excess electrons and the electrons of the monomers make substantial contributions to the electron binding energies.[92, 93, 94, 95, 108, 109] This suggests that the polarization potentials used in the model potential approaches implicitly include long-range correlation effects.

3.2 THEORETICAL CONSIDERATIONS

3.2.1 General background

The role of electrostatics, in particular, long-range dipole potentials, in the binding of excess electrons to molecules and clusters, has been addressed in numerous theoretical studies.[108, 109, 119, 120, 121, 122, 123, 124, 125, 126] Here, we note that, within the context of the Born-Oppenheimer approximation,[127] any molecule or cluster with a dipole moment greater than

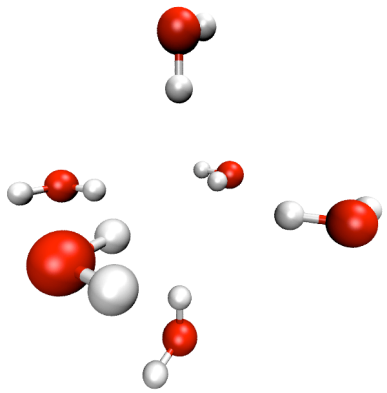

Figure 15: Octahedral arrangement of six water monomers in a model cavity of the solvated electron proposed by Feng *et al.*[87]

1.625 D can bind an excess electron giving a so-called dipole-bound anion.[122, 123, 124, 125] When corrections to the Born-Oppenheimer approximation are included, the critical dipole for binding the excess electron is found to depend on the moments of inertia but, as a rule-of-thumb, can be taken to be about 2.2 D.[126]

The electrostatic potential associated arrangements of polar molecules with zero or near zero dipole moments may also be able to bind an excess electron. The $(H_2O)_6$ species depicted in 15, which represents such an arrangement, has been proposed as a model for the first shell of water molecules of e^-_{aq}.[87]

Although electrostatic interactions clearly play a crucial role in the binding of excess electrons to polar molecules and their clusters, they are far from the complete story. It has long been known that the "excluded volume" effect due to the valence electrons of the molecules causes a reduction of the EBEs compared to those expected based on a purely electrostatic potential.[119, 120] More recently, it was recognized that electron correlation effects,[108, 109] in particular,[108, 109] dispersion-type interactions between the weakly bound excess electron and the more tightly bound electrons of the polar molecules, also

significantly impact the binding of the excess electron. That such dispersion interactions could make a sizable contribution to the EBE follows from the large polarizability of the weakly bound electron. In classical force fields, dispersion interactions are generally handled by adding C_6/R^6, and sometimes higher-order dispersion terms. However, due to the spatially extended nature of the weakly bound electron, this approach cannot be used to account for the dispersion contributions to the electron binding energies of $(H_2O)_n^-$ clusters. The Drude model developed in our group[128, 129, 62, 63, 130, 120] does account for the dispersion contributions to the EBEs, and, as will be shown below, so do models that allow for polarization of the water monomers by the excess electron. *Ab initio* MP2 and coupled-cluster calculations do incorporate long-range dispersion interactions and, thus, are valuable for testing model potential approaches for describing $(H_2O)_n^-$ ions. It is useful, therefore, to briefly review *ab initio* approaches for calculating EBEs.

3.2.2 *Ab initio* treatment of $(H_2O)_n^-$ clusters

Through second-order, the EBE, here taken as positive for a stable anion, may be written as

$$\mathrm{EBE} = E_{\mathrm{KT}} + \Delta E_{\mathrm{relax}} + \Delta E_2, \tag{3.1}$$

where E_{KT}, $\Delta E_{\mathrm{relax}}$, and ΔE_2 represent the Koopmans' theorem (KT),[131] relaxation, and second-order correlation contributions to the electron binding energy, respectively. E_{KT} is given by the negative of ϵ_{LUMO}, the energy of the lowest unoccupied molecular orbital of the neutral cluster; $\Delta E_{\mathrm{relax}}$ is defined as the difference between the ΔHF and KT binding energies; and ΔE_2 is given by the difference of the ΔHF and ΔMP2 binding energies, where

$$\Delta\mathrm{HF} = E_{\mathrm{HF}}(\mathrm{neutral}) - E_{\mathrm{HF}}(\mathrm{anion}) \tag{3.2}$$

and

$$\Delta\mathrm{MP2} = E_{\mathrm{MP2}}(\mathrm{neutral}) - E_{\mathrm{MP2}}(\mathrm{anion}), \tag{3.3}$$

where HF and MP2 denote Hartree Fock and second-order Møller-Plesset perturbation theory, respectively.

For many molecules and their clusters, ϵ_{LUMO} is positive, implying that the excess electron is unbound at the KT level of theory. However, for water clusters with the monomers arranged so as to generate a sufficiently large region where the potential is sufficiently attractive, an excess electron binds even at the KT level, provided a suitably flexible basis set is employed. For small clusters the relaxation corrections are generally much less important than the correlation corrections to the EBEs.[128, 129, 120]

The second-order correlation correction to the EBE can be further decomposed into a contribution associated with the redistribution of the charge of the neutral molecule and a contribution due to dispersion interactions between the excess electron and the electrons of the monomers.[108] The former contribution, hereafter referred to as charge renormalization, acts so as to reduce the EBE, primarily as a result of the reduction of the dipole moment of the water monomer from about 1.93 to 1.86 D in going from the Hartree-Fock to the MP2 approximation (with suitably flexible basis sets). The second-order dispersion corrections are necessarily positive (in the adopted sign convention). *Ab initio* calculations on small water clusters have shown that the dispersion contributions to the EBEs are generally much greater in magnitude than the charge renormalization contributions.[109] Hence, the net effect of the second-order corrections is to increase the EBEs.[109]

Two of the most commonly used approaches for accounting for correlation corrections beyond second order to the EBEs are the CCSD(T)[110] or EOM-CCSD[132] methods. The electron binding energy at the CCSD(T) level of theory is given by:

$$\Delta\mathrm{CCSD(T)} = E_{\mathrm{CCSD(T)}}(\mathrm{neutral}) - E_{\mathrm{CCSD(T)}}(\mathrm{anion}), \tag{3.4}$$

with the difference between the ΔCCSD(T) and ΔMP2 results providing an estimate of the contribution of correlation corrections beyond second order. The EOM-CCSD method calculates the electron binding energy directly, rather than from an energy difference, and is applicable even in cases that the MP2 and CCSD(T) methods may not be reliable due to the failure of the excess electron to bind in the KT or Hartree-Fock approximations.

Excess electrons in $(H_2O)_n^-$ clusters occupy very extended orbitals, with relatively little charge density in the valence region of the molecules. As a result, flexible basis sets containing several sets of diffuse functions are required to converge the EBEs of the excess

electron states. The requirements for choosing such basis sets have been described in prior publications and will not be repeated here.[133, 109, 108] The *ab initio* calculations carried out in the course of this study have used sufficiently flexible basis sets for which the electron binding energies are close to converged with respect to the basis set. The Hartree-Fock, MP2, and CCSD(T) calculations were performed using the Gaussian 03 program,[44] and the EOM-CCSD calculations were carried out using the ACES program.[134]

3.2.3 Quantum Drude model

Over the past several years our group has introduced a quantum Drude model for describing excess electrons interacting with clusters of water and other polar molecules.[128, 129, 62, 63, 130, 120] The quantum Drude model combines the DPP classical force field for the water-water interactions with a model Hamiltonian, H_{D}, for the electron-water interaction.[19] The classical force field defines the energy of the neutral cluster and also provides the electrostatic potential V_{es} for the excess electron. As illustrated in figure 16, a Drude oscillator consists of two charges, a fixed $+q$ charge and a mobile $-q$ charge, coupled harmonically through a force constant k.[135] Here we have assumed that the polarizability is isotropic, a reasonable approximation for water. The polarizability of a Drude oscillator, α_{D} is given by q^2/k, chosen to equal the experimental value of the isotropic polarizability of the water monomer, *i.e.*, 9.745 a.u.^{3}.[53] The fixed $+q$ charge of a Drude oscillator is located at the M site of the DPP model, displaced 0.25 Å from the O atom, as shown in Fig 16.

In principle, the Drude oscillators can be used to describe the dispersion and induction interactions between the monomers as well as between the excess electron and the monomers, allowing for a fully self-consistent treatment. However, we have found that it is adequate to adopt a computationally faster approach in which the water-water induction and dispersion interactions are described by the water force field, with the Drude oscillators (one on each monomer) being employed to describe only the dynamical response of the electron distribution of the water molecules to the excess electron.

In the DPP water model[19] the static charge distribution of each monomer is represented by three point charges and induction is treated *via* three mutually interacting point

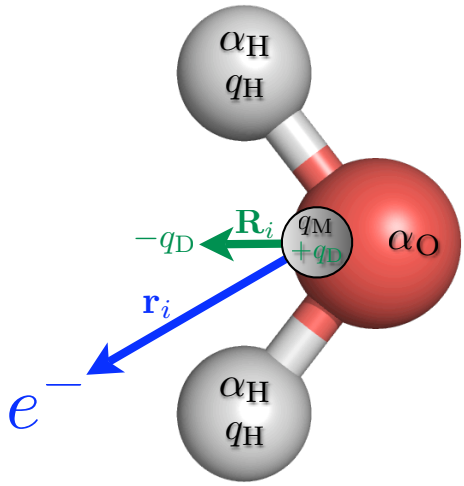

Figure 16: Schematic of the monomer parameters and interactions in the Drude/DPP model. Position of charges and polarizabilities for the DPP water model[19] are in black. In blue is the distance from the M-site to the excess electron. In green are the two harmonically coupled charges for the Drude oscillator.

polarizable sites. Intermonomer dispersion is described by means of damped C_6/R^6 terms, and short-range exchange-repulsion interactions between the monomers are modeled by exponential contributions. The key parameters for the DPP model are summarized in Fig 16.

The Drude model Hamiltonian, H_{D}, includes the electronic Hamiltonian, H_e, the Hamiltonian for the collection of Drude oscillators, H_{osc}, and a term describing the coupling between the electron and the oscillators. The potential energy portion of H_e includes V_{es}, which describes the interaction of the excess electron with the point charges, used to model the fixed charge distributions of the monomers, as well as with the induced dipoles from intramonomer induction, and V_{rep}, which describes the short-range repulsion and exchange interactions between the excess electron and the valence electron distributions of the monomers. In this work, the repulsive potential of Ref. [128] is employed rather than the simpler, more approximate, repulsive potential of Ref. [129].

In summary, the Drude Hamiltonian for the interaction of an excess electron with N

monomers is given by

$$H_{\mathrm{D}} = H_e(\mathbf{r}) + \sum_{i=1}^{N} h_{\mathrm{osc}}(\mathbf{R}_i) + \sum_{i=1}^{N} V_{e,\mathrm{osc}}(\mathbf{r}, \mathbf{R}_i), \tag{3.5}$$

where

$$H_e = -\frac{\hbar^2}{2m_e}\nabla_e^2 + V_{\mathrm{es}} + V_{\mathrm{rep}}, \tag{3.6}$$

and

$$h_{\mathrm{osc}} = -\frac{\hbar^2}{2m_D}\nabla_D^2 + \frac{1}{2}k_D\left(X_i^2 + Y_i^2 + Z_i^2\right), \tag{3.7}$$

and

$$V_{e,\mathrm{osc}} = q_D \frac{\mathbf{r}_i \cdot \mathbf{R}_i}{r_i^3} f(r_i). \tag{3.8}$$

In Eqs. 3.5-3.8, $\mathbf{r}$ is the collection of coordinates describing the interaction of the excess electron with the permanent point charges, the induced point dipoles, and the repulsive sites in the pseudopotentials, $\mathbf{r}_i$ is the vector from the electron to oscillator i, $R_i = (X_i, Y_i, Z_i)$ is the displacement vector of Drude oscillator i, and $f(r)$ is a function that damps out the unphysical short-range behavior of the coupling term and is taken to be $1 - exp(-br^2)$. It should be noted that Eq. 3.8 retains only the leading term resulting from the separation of the pair of charges associated with a Drude oscillators.

In solving for the energy levels of H_{D}, we make use of a product basis set, consisting of s and p Gaussian-type (GTO) functions for the excess electron and a "minimal" basis set of the four lowest harmonic oscillator states $|000\rangle, |100\rangle, |010\rangle, |001\rangle$ for each oscillator. The basis set for the excess electron, as described in Ref. [120], consists of a single s-type GTO centered on each H atom, a $1s1p$ set of GTOs centered on the midpoint between the two H atoms of each monomer, and a $5s4p$ set of GTOs located at the center of mass of the cluster. These electron and oscillator basis sets are adequate for describing both surface bound and interior bound states of the excess electron for the clusters considered here (although, to obtain fully converged results, still larger electronic basis sets would be required for a few of the clusters).

In our applications of the quantum Drude model to $(H_2O)_n^-$ clusters, the principal approach for evaluating the energy associated with H_{D} is the single-plus-double-excitation configuration interaction (CI) approximation, where the double excitations are restricted to

configurations that involve simultaneous excitation of the excess electron and of one of the Drude oscillators. We also report for the model potential approaches EBEs from a KT-like approximation, which neglects the coupling of the excess electron to the Drude oscillators, as well as from a second-order perturbation theory treatment. These are included primarily for illustrating the different rates of convergence of the EBEs with the order of the interaction in the Drude model and *ab initio* approaches.

The Drude Hamiltonian contains two free parameters, σ and b, both of which are determined by fitting to *ab initio* results for the water dimer. The σ parameter scales the repulsive potential, and is chosen so that for the water dimer the KT EBE from the model potential calculation matches that from a large basis set *ab initio* Hartree-Fock calculation on the neutral molecule. The b parameter, which controls the damping of the electron-Drude coupling, is adjusted so that the electron binding energy of the water dimer, calculated using the Drude model in conjunction with the CI method, matches that (41 meV) from large basis set *ab initio* CCSD(T) calculations. This gives a value of $b = 0.9312$ a.u.$^{-2}$.

3.2.4 Adiabatic approximation

Up to this point the choices of q_{D} and m_{D} have not been specified. In our applications of the Drude model to water clusters we have chosen $q_{\mathrm{D}} = |e^-|$ and $m_{\mathrm{D}} = m_e$. With this choice, the excitation energy of the Drude oscillator is 8.7 eV, a reasonable value for an effective valence excitation energy of the water monomer. For most of the clusters considered here, the excess electron binds by at most 1.1 eV, almost an order of magnitude smaller than the excitation energy of a Drude oscillator, suggesting the possibility of an adiabatic separation between the excess electron and the Drude oscillators. To illustrate how this separation is accomplished, we consider the case of an excess electron interacting with a single Drude oscillator. The extension to multiple oscillators is straightforward.

In the adiabatic approximation, the Hamiltonian for the fast degrees of freedom (here associated with the Drude oscillator),

$$H_f(\mathbf{r};\mathbf{R}) = h_{\mathrm{osc}}(\mathbf{R}) + V_{e,\mathrm{osc}}(\mathbf{r};\mathbf{R}) \tag{3.9}$$

depends only parametrically on the position $\mathbf{r} = (x, y, z)$ of the clamped excess electron. The eigenvalues U_j of H_f, when combined with the electrostatic and electron-molecule repulsive terms, give potential energy surfaces for the motion of the excess electron. Provided that the non-adiabatic couplings between the ground and excited potential energy surfaces are small, a Born-Oppenheimer-like treatment of the excess electron on the ground state adiabatic surface, U_0, should closely reproduce the electron binding energies from the "full" Drude model.

To determine the potential $U_0(\mathbf{r})$, the matrix elements of H_f are evaluated in terms of the eigenfunctions $|n\rangle$ of h_{osc}

$$h_{\text{osc}}\left(\mathbf{R}\right)|n\rangle = E_n|n\rangle \tag{3.10}$$

where $n = (n_x, n_y, n_z)$ is a collective index of the quantum numbers of the three-dimensional harmonic oscillator, and $E_n = (2n_x + 2n_y + 2n_z + 3)\epsilon_{\text{D}}$, with $\epsilon_{\text{D}} = 0.5\hbar\omega_{\text{D}}$. In this basis set the matrix elements of H_f are

$$\langle n|H_f|m\rangle = E_n\delta_{n,m} + \frac{q_D}{r^3}f(r)\sum_{n,m}\left(x\langle n|X|m\rangle + y\langle n|Y|m\rangle + z\langle n|Z|m\rangle\right) \tag{3.11}$$

with the matrix elements contributing to the first term in parenthesis being given by

$$\langle n|X|m\rangle = \langle n_x n_y n_z|X|m_x m_y m_z\rangle = \begin{cases} \sqrt{\frac{n_x+1}{2\omega_{\text{D}}m_{\text{D}}}} & n_x = m_x - 1, n_y = m_y, n_z = m_z \\ \sqrt{\frac{n_x}{2\omega_{\text{D}}m_{\text{D}}}} & n_x = m_x + 1, n_y = m_y, n_z = m_z \\ 0 & \text{otherwise} \end{cases} \tag{3.12}$$

with analogous expressions for the matrix elements of Y and Z.

With the "minimal" basis set described above for the Drude oscillators, the matrix representation of H_f is

$$\mathbf{H}_f = \begin{pmatrix} 3\epsilon_D & xv(r) & yv(r) & zv(r) \\ xv(r) & 5\epsilon_D & 0 & 0 \\ yv(r) & 0 & 5\epsilon_D & 0 \\ zv(r) & 0 & 0 & 5\epsilon_D \end{pmatrix} \tag{3.13}$$

where

$$v(r) = \frac{q_D}{r^3}f(r)\sqrt{\frac{\hbar}{2\omega_D m_D}}. \tag{3.14}$$

The lowest eigenvalue of H_f is

$$U_0(r) = 4\epsilon_D - \sqrt{\epsilon_D^2 + \frac{\hbar q_D^2}{2\omega_D m_D r^4} f^2(r)}. \tag{3.15}$$

After subtracting the zero-point energy E_0, this gives the adiabatic potential

$$V_{\rm ad}(r) = \epsilon_D - \sqrt{\epsilon_D^2 + \frac{\epsilon_D \alpha_D}{r^4} f^2(r)} \tag{3.16}$$

For large r, a Taylor series expansion in powers of r^{-4} gives

$$V_{\rm ad}(r) = -\frac{\alpha_D}{2r^4} f^2(r) + \frac{\alpha_D^2}{8\epsilon_D r^8} f^4(r) - \cdots \tag{3.17}$$

the leading term of which is the asymptotic form of the polarization potential multiplied by the square of the damping function. This result demonstrates that the $\alpha/2r^4$ polarization potential commonly employed in one-electron models for excess electrons interacting with molecules and clusters does include long-range (*i.e.*, dispersion-like) correlation effects. This has been demonstrated previously in other contexts and using different derivations. For example, it has been shown that the asymptotic form of the potential describing the interaction of the outer electron and the cation core of spherical atoms such as Na contains a $-0.5\alpha_I/r^4$ term, where α_I is the polarizability of the ion core.[136] In fact, this is exploited in the polarizable core pseudopotentials of Stoll and co-workers.[137] Similarly, the asymptotic form of the correlation potential for electron-atom and electron-molecule scattering contains an analogous term where the polarizability is that of the neutral target.[138]

Although the use of polarization potentials to describe correlation effects is well documented in the literature, it is not fully appreciated in the quantum chemistry community. The key to understanding the recovery of electron correlation effects through the use of a polarization potential is to recognize that there is a fundamental difference between the interaction of a point charge and the interaction of an excess electron with a polarizable atom or molecule. In both cases the response of the atom or molecule to the charge can be described by allowing for single excitations of the atom or molecule. However, in the case of the excess electron, the excitations of the "target" generate a polarization term which is then added to the potential in the one-electron Schrödinger equation for the excess electron. Even though the above derivation and discussion make it clear that polarization potential models

do include correlation effects, it remains to be established whether polarization potential models can accurately account for the EBEs for both surface and interior and surfaces states and for both small and large clusters.

In this work we consider four adiabatic potential models: (1) the full adiabatic potential given by Eq. 3.16, with f chosen to be $(1 - exp(-br^2))$, (2) the leading term in the Taylor series expansion in Eq. 3.17, with f again chosen to be $(1-exp(-br^2))$, (3) the full adiabatic potential give by Eq. 3.16, but with f chosen to be $(1 - exp(-br^3))$, and (4) $\alpha_{\rm D}/(r^2 + r_c^2)^2$, where r_c is a cutoff parameter. These adiabatic potentials are combined with the electrostatic and repulsive terms of Eq. 3.6 to give four one-electron model Hamiltonians designated PM1, PM2, PM3, and PM4, respectively. For each water cluster considered, the electron binding energies were calculated for each of these models using the same Gaussian basis set for the excess electron as used in the Drude model calculations as well as using a discrete variable representation (DVR) with sine-type particle-in-the-box functions. In general, the DVR calculations give electron binding energies close to those obtained using the GTO basis set, and, for that reason, only the latter results are reported here.

An issue that arises in the use of the polarization potential models concerns the choice of the damping or cutoff parameters. One might anticipate that the b parameter used in the Drude model could simply be carried over to the PM1 and PM2 models. However, with this choice, the PM1 and PM2 models significantly overbind the excess electron for all clusters considered. This may be a consequence of the integrands in the integrals encountered in the polarization potential models more heavily weighing small r values than in the Drude model. To solve the overbinding problem, the damping (or cutoff) parameters in the various polarization potential models have been adjusted so that the electron binding energies for the water dimer calculated using these models reproduce the 41 meV value from large basis set *ab initio* CCSD(T) calculations. This approach gives $b = 0.214$ and 0.180 a.u.$^{-2}$ for the PM1 and PM2 models, respectively, $b = 0.0915$ a.u.$^{-3}$ for the PM3 model, and $r_c = 1.684$ a_0 for the PM4 model. The former two values differ by about a factor of three from the corresponding values for the Drude model.

Figure 17 displays the polarization potentials of the PM1, PM2, PM3, and PM4 models together with the MP2 level *ab initio* polarization potential. The latter was obtained by

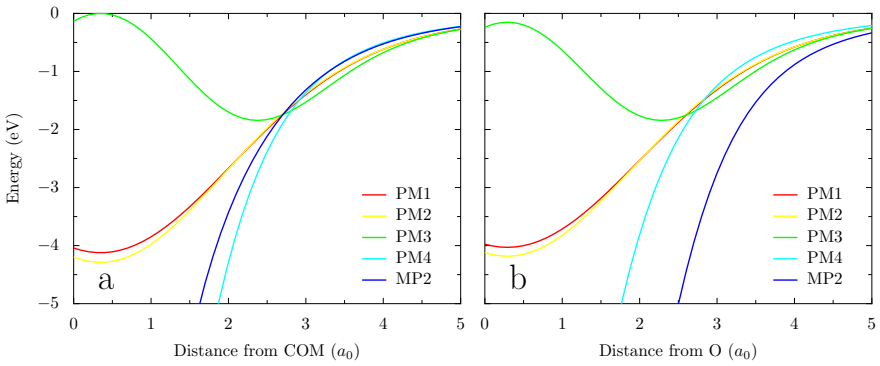

Figure 17: Comparison of the four polarization models with MP2 calculations (a) along the HOH bisector with the hydrogen pointing along the positive axis and (b) along OH bond vector with the hydrogen pointing along the positive axis. The MP2 potential was calculated by subtracting the electrostatic energy in the presence of a negative point charge ($-e$) from the total energy.

performing MP2/aug-cc-pVTZ calculations on H_2O in the presence of negative ($-e$) point charge, and subtracting from the resulting energies the purely electrostatic (neglecting induction) contributions. In each case the potential is plotted along the HOH bisector as well as along an OH bond of a monomer.

There are several important conclusions that can be gleaned from examination of the curves shown in Figure 17. For $r \gtrsim 2$ Å (measured from the O atom), the polarization potentials associated with the various PMx models are in fairly good agreement with each other and with the MP2 polarization potential, although it is clear that there is appreciable anisotropy in the *ab initio* polarization potential which, of course, is not recovered with the model potentials that employ only a single, isotropic polarizable site. For $r \lesssim 2$ Å, the various polarization potentials differ significantly from one another and are significantly less attractive than the MP2 polarization potential. However, at these short distances, the repulsive term makes a sizable contribution to the net potential, weakening the sensitivity of the EBE to the precise form of the damping of the polarization potential. In addition, the exact potential for the interaction of an excess electron with a water monomer would

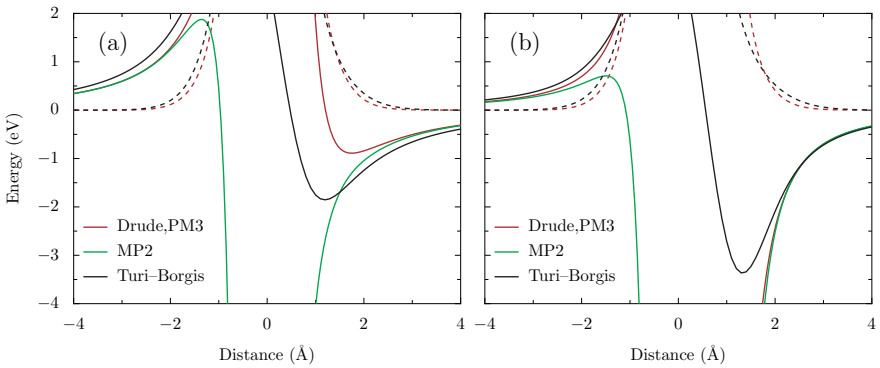

Figure 18: Electrostatic (solid) and repulsion potentials (dashed) for the Drude/DPP polarization models and TB plotted (a) along the HOH bisector with hydrogens pointing along the positive axis and (b) along OH bond vector with the hydrogen pointing along the positive axis.

include exchange-induction and charge-penetration effects which are expected to be important at these small r values. Although the model potentials do not include explicit terms for describing these short-range effects, they are incorporated in an effective manner through the adjustment of the damping (or cutoff) parameter to reproduce the *ab initio* CCSD(T) EBE of the water dimer.

Fig. 17 also includes the polarization potential employed in the Turi-Borgis (TB) electron-water potential, which has been used in several recent simulations of $(H_2O)_n^-$ clusters as well as of excess electrons in bulk water.[104, 105, 83] From this figure, it is seen that the TB polarization potential is much weaker than the *ab initio* and PMx polarization potentials. Fig. 18 displays the repulsive and electrostatic potentials employed in the PMx and Turi-Borgis model potentials together with the MP2-level electrostatic potential. From this figure it is seen that the repulsive potentials in the two models are very similar. In contrast, the electrostatic potentials differ appreciably, with that associated with the Turi-Borgis model being more attractive on the H-end of the molecule. This is a consequence of the TB model being based on the SPC force field, which employs enhanced charges and gives for the water monomer a dipole moment of 2.3 D, about 25% larger than the experimental gas-phase value.

In water clusters, the importance of intramolecular induction depends on the geometrical arrangement of the monomers, and, as a result, the net electrostatic potential experienced by the excess electron can be either under- or overestimated, depending on the geometry, when employing a non-polarizable force field with enhanced charges.

4.0 RESULTS OF THE DRUDE MODEL FOR WATER CLUSTER ANIONS

Manuscript in preparation Thomas Sommerfeld, Albert DeFusco and Kenneth D. Jordan

4.1 INTRODUCTION

In the present study *ab initio* electronic structure methods are employed and the quantum Drude model (QDM) developed in our group[128, 129, 62, 63, 130, 120] to elucidate the role of correlation effects in the binding of excess electrons to water clusters. This model incorporates the induction and dispersion interactions between the excess electron and the electrons of the monomers by use of quantum Drude oscillators. In essence, this is a course-grained approach that models the dynamical response of the ten electrons of each monomer by two point charges, coupled harmonically. Unlike other model potential approaches, the quantum Drude model explicitly accounts for correlation effects, but at a fraction of the computational cost of *ab initio* methods. It will be shown below that the quantum Drude model combined with an adiabatic approximation to derive one-electron polarization models, thereby providing insight into how such models incorporate correlation effects. The electron binding energies calculated using the resulting polarization models are compared with those from *ab initio* calculations and from the full Drude model in order to determine the range of validity of one-electron polarization models for $(H_2O)_n^-$ clusters. The test cases include clusters ranging from $(H_2O)_6^-$ to $(H_2O)_{45}^-$ in size. Both surface-bound and interior- (or cavity)-bound species are considered.

As alluded to in the previous Chapter, there are subtle differences between individual contributions to the EBEs obtained from the model potential and *ab initio* approaches.

In addition, for some of the clusters considered there are problems caused by inappropriate zeroth-order wavefunctions. We find it useful, therefore, to start this chapter with a brief consideration of these issues. We then turn to the results for several isomers of the $(H_2O)_6^-$, which is the largest water cluster for which there are electron binding energies from large-basis set CCSD(T) calculations,[111] several isomers of $(H_2O)_{20}^-$ and $(H_2O)_{24}^-$ that were studied previously by Herbert and Head-Gordon,[93, 94] and two isomers of $(H_2O)_{45}^-$ that were studied by Turi and Rossky.[105] This is followed by a brief examination of the low-lying excited states predicted by the model potential approaches. The following chapter contains an analysis of the isomer populations of $(H_2O)_7^-$ obtained from Drude model Monte Carlo simulations.[60]

4.2 GENERAL CONSIDERATIONS

Overall, all four PMx models give similar values of the EBEs, with the agreement with the Drude model results being slightly better for the PM3 model. We note also that the PM4 model, which uses a cutoff rather than a damping function in the polarization potential, performs more poorly than the other models. For this reason, only the PM3 results will be considered in the ensuing discussion.

Table 8 summarizes the calculated EBEs of the ground state anions of the test systems. Results are reported for the Drude, PM3, and TB models, and, for the $n \leq 6$ clusters, from *ab initio* calculations. In the case of the Drude model, the EBEs are reported for the electrostatic plus repulsion (ES+rep), second-order perturbation theory, and single-plus-double excitation CI levels of theory. The second-order corrections are further separated into induction and dispersion contributions. The ES+rep method is a KT-like approximation as it neglects the Drude oscillators in the Hamiltonian given in Eq. 3.5. It is important to note, however, that the atomic charges employed in the model Hamiltonian have been chosen so as to reproduce the experimental dipole moment of the gas-phase monomer, whereas *ab initio* Hartree-Fock calculations give a dipole moment for the monomer that is about 15% too large. In *ab initio* approaches, such as MP2 or CCSD(T), that are built on a Hartree-Fock wavefunction, the

Table 8: Electron binding energies (meV) for $(H_2O)_2^-$, $(H_2O)_6^-$, $(H_2O)_{20}^-$, $(H_2O)_{24}^-$, and $(H_2O)_{45}^-$. For $(H_2O)_6^-$ isomers, relative energies appear in parenthesis.

		Drude						TB			*Ab Initio*			
Cluster	μ(D)	Es+rep	Ind	Disp	2nd order	CI	PM3	Es+rep	pol.	total	KT	HF	MP2	CCSD(T)[a]
2[b]	3.9	6	0	9	15	41	41							41
6A	9.4	171	25	135	331	451	453	272	68	340	286	290	404	470
6B	8.5	180	37	189	406	569	592	407	117	524	312	368	543	610
6C	9.2	123	17	102	242	374	384	221	64	285	185	199	279	340
6D	12.2	129	10	104	243	332	330	158	41	198	230	247	333	380
6E	0	60	48	276	384	565	614	478	166	644	194	269	494	550
6F	0	−4	0	8	4	835	932	175	239	414	145	366	800	779
														(s-MP2)[a]
20A	24.9	566	81	244	891	1074	1110	656	137	793		883	1083	(1085)
20B	18.8	432	77	221	730	910	946	531	131	662		723	908	(925)
20C	14.5	252	58	180	490	670	705	324	114	438		497	657	(706)
20D	14.2	183	40	145	368	545	581	246	99	345		379	516	(586)
20E	2	−4	0	1	−3	48	78	0	16	16		−51	−22	(118)
20F	0.1	7	1	82	89	372	477	0	159	159		93	227	(421)
24A	0	−5	0	1	−4	764	1028	−17	285	268		80	576	(682)
24B	0	−5	0	1	−4	91	142	5	26	31		−35	31	(175)
24C	0	−5	0	1	−4	447	701	−8	29	21		−35	4	(302)
24D	0	−5	0	2	−3	999	1290	11	464	475		254	793	(805)
24E	0	−3	0	13	10	237	267	97	46	143		49	136	(316)
45A	9.2	697	1159	900	2766	2508	2861	1640	716	2356				
45B	22	742	158	313	1213	1350	1480	775	211	986				

[a]CCSD(T) results for the $(H_2O)_6^-$ isomers and s-MP2(BHLYP) results for the $(H_2O)_{20}^-$ and $(H_2O)_{24}^-$ isomers.

[b]Geometry optimized with MP2/aug-cc-pVDZ+5s4p

correlation contribution to the EBE includes terms that correct for the deficiencies of the Hartree-Fock charge distribution. In contrast, the effect of charge-renormalization on the EBEs is incorporated in the zeroth-order energy in the Drude model. As a result, the EBEs from the ES+rep and second-order Drude model calculations are not directly comparable to the EBEs from *ab initio* KT or MP2 calculations. The Drude model CI and *ab initio* CCSD(T) EBEs, however, are directly comparable. As will be discussed below, for the six $(H_2O)_6^-$ isomers, the changes in the EBEs in going from MP2 to CCSD(T) calculations are relatively small, making comparison with the results of *ab initio* MP2 calculations a viable alternative for testing the model potentials for larger clusters for which *ab initio* CCSD(T) calculations are not feasible.

Examination of Table 8 reveals that for most of the clusters with zero or near zero dipole moments, both the Hartree-Fock and ES+rep approaches fail to bind or only weakly bind the excess electron, with the failure to bind the excess electron being more prevalent with the ES+rep method due to the weaker electrostatics in this approach. For these clusters, perturbative approaches based on the Hartree-Fock or ES+rep wavefunctions prove to be inadequate. The Drude model CI and the polarization model approaches do not suffer from this problem because they do not depend on the validity of a zeroth-order wavefunction. Indeed, both Drude model CI and polarization model calculations predict the excess electron to bind to all clusters considered.

It should be noted that, even in those cases where the electron fails to bind in the ES+rep approximation, electrostatic interactions play an important role in its binding in the Drude model CI or polarization model approaches. This can be seen by carrying out Drude model CI calculations with the permanent charges on the water monomers set equal to zero. Such calculations fail to bind the excess electron for most of the water clusters considered, thereby establishing the importance of electrostatic interactions for the electron binding.

For clusters with sizable dipole moments, the excess electron acquires a significant binding energy in both the ES+rep and Hartree-Fock approaches. However, even for these species, electron correlation effects play an important role, typically leading to increases in the EBEs by a factor of 2-3 in the Drude model and by 60-80% in the *ab initio* calculations. Correlation corrections beyond second order are very important in the Drude model, in some clusters

being comparable to the second-order corrections, whereas they are much smaller (5-10%) in the *ab initio* calculations. The different behavior of the correlation corrections in the Drude model and *ab initio* approaches is due to the partial cancellation between charge renormalization and other contributions to the correlation energy in the latter. As a result, *ab initio* MP2 calculations are useful for assessing the reliability of model potential approaches for calculating EBEs, at least in those cases where there is appreciable electron binding in the KT approximation. (This has been noted previously by Herbert and Head-Gordon.[93, 94]) This is an important observation since the MP2 method can be applied to much larger clusters than can the CCSD(T) method.

4.3 RESULTS FOR $(H_2O)_6^-$

The six $(H_2O)_6^-$ isomers considered, are shown in Fig. 19. Of these, four (6A-6D) have large dipole moments and surface-bound excess electron states, and two (6E and 6F) have no net dipole moment. 6E consists of two trimers with the three free OH groups of each trimer being pointed toward the other trimer generating a region with a strongly attractive electrostatic potential between the trimers. 6F is the model for the first salvation shell of e_{aq}^- mentioned in the previous chapter and depicted in Fig. 15. 6A-6E are true minima on the $(H_2O)_6^-$ potential energy surface, while 6F is not a local minima.

In 6F, the O atoms of water molecules are in an octahedral arrangement, with one H atom of each monomer pointed toward the center of the cavity. The distance between the O atoms is taken to be 6.1 Å, the diameter of the cavity associated with e_{aq}^-. Fig. 19 also displays for the $(H_2O)_6^-$ species the charge distributions of the excess electron as described by the Drude model CI calculations. In this figure, and in the corresponding figures shown below for the larger clusters, contours enclosing 50 and 90% of the electron density are shown. For all six $(H_2O)_6^-$ species the Drude model CI and PM3 polarization models give EBEs close to the CCSD(T) values, with the average absolute difference of the model potential EBEs from the corresponding CCSD(T) values being only about 5%. The largest differences ($\sim$ 14%) are for the chain isomer 6D, for which the Drude CI and PM3 approaches underestimate the

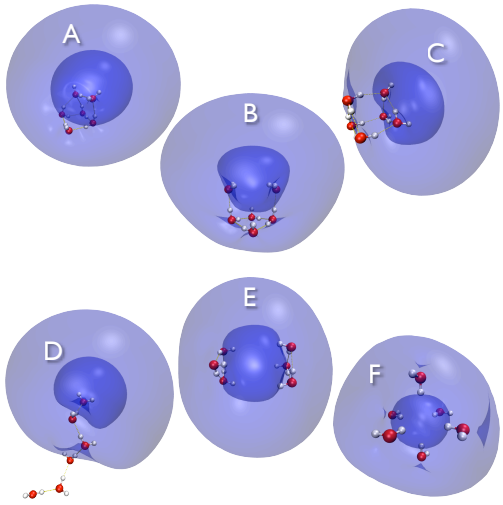

Figure 19: Six isomer of $(H_2O)_6^-$. A-E have been identified by M. Gutowski. For each 50 and 90% excess electron density contours as computed with the Drude model are plotted. Isomer F is a solvated electron cavity proposed by Feng *et al.*[87]

EBE. The larger errors in the EBEs calculated using the model potential approaches for 6D are due mainly to our locating the off-atom $5s4p$ set of functions at the center of mass of the cluster which is far from the excess electron, rather than to an inherent deficiency in the model potentials.

The changes in the EBEs in going from the KT to the Hartree-Fock approximation are relatively small for 6A - 6D, with sizable dipole moments, but are sizable for 6E and 6F (39 and 152% respectively), which have no net dipole moment and for which the excess electron is nominally cavity bound. (Obviously, for such small clusters, much of the excess electron distribution is located outside the cavity as can be seen from Fig. 19.) The inclusion of electron correlation effects using *ab initio* methods leads to 53-71% increases in the electron binding energies for 6A-6D and to about 100% increases for 6E and 6F, with most of the correlation contribution being recovered at the MP2 level of theory. As discussed in the previous chapter, both correlation contributions beyond second order and the net correlation contributions are much larger in the Drude model than in the *ab initio* calculations. It is for this reason that a CI rather than a perturbative approach has been adopted in our

Table 9: Contributions the EBE for the 6 $(H_2O)_6^-$ isomers. KE is the kinetic energy, ES the electrostatic expectation value, and Repulsion is the repulsion expectation value. Correlation is defined as the difference between the sum of reported contributions and CI EBE.

	6A		6B		6C		6D		6E		6F	
Contribution	KT	CI	KT	CI	KT	CI	KT	CI	KT	CI	KT	CI
KE	345	654	411	805	252	580	255	514	426	846	12	1470
ES	−578	−918	−684	−1116	−418	−763	−433	−716	−621	−1109	−12	−2110
Repulsion	63	256	93	329	43	256	49	183	134	347	4	654
Sum	−171	−8	−180	17	−123	82	−129	−18	−60	84	4	253
Correlation	—	−443	—	−619	—	−465	—	−312	—	−649	—	−1032
Total[a]	−171	−451	−180	−592	−123	−383	−129	−330	−60	−565	430	3.2
Rg[b]	6.72	4.31	6.16	3.89	7.91	4.72	9.28	5.27	7.18	3.68	43	3.23

[a]It is noted here that due to the sign of the individual contributions, a bound anion is a negative number.
[b]Radius of gyration calculated as $Rg = \sqrt{\langle r^2 \rangle - \langle r \rangle^2}$.

applications of the Drude model. 6F is particularly interesting, in that, even though it does not bind the excess electron in the ES+rep and 2nd-order Drude model treatments, the Drude model CI calculations give an EBE close to the ab initio CCSD(T) result. We note also that, in the Drude model calculations on the 6A-6E anions, the second-order dispersion corrections to the EBEs are much larger than the second-order induction corrections.

Additional insight into the relative importance of various contributions to the EBEs is provided by Table 9 which reports for the six $(H_2O)_6^-$ isomers the kinetic energy, electrostatic, and repulsion contributions calculated using the ES+rep and Drude model CI approaches. (The PM3 results are close to those of the Drude CI calculations, and, for that reason, have not been included in the Table.) For the CI calculations, the correlation energy contributions to the EBE are also reported. For all six isomers, the kinetic energy contribution roughly doubles upon inclusion of the correlation contributions, (with either the Drude or PM3 models), consistent with the excess electron being much more localized in the calculations including correlation effects.

Table 9 also includes values of the radius of gyration $Rg = \sqrt{\langle r^2 \rangle - \langle r \rangle^2}$ calculated at the ES+rep and Drude-CI levels of theory. (The Rg values for the PM3 model are

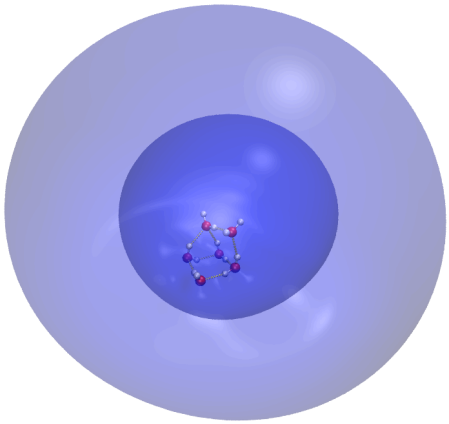

Figure 20: The 90% contour for ES+rep and CI approximations are plotted. The larger, light blue, contour is the ES+rep.

very close to the corresponding Drude CI values.) The *Rg* values are typically about 3 Å smaller for the Drude-CI and PM3 than for the ES+rep wavefunctions, again consistent with large contractions of the excess electron distributions due to inclusion of correlation effects. This is also seen from Figure 20 where the change distributions of the excess electron of 6A as described by the ES+rep and Drude CI approximations are plotted. The origin of the contraction is obvious in the polarization model approach; namely, the inclusion of the polarization term adds an additional attractive short-range (compared to the electrostatics) term in the net electron-water potential. A similar contraction of the electron density due to inclusion of correlation effects is also found in *ab initio* calculations, although we are unaware of any published papers on $(H_2O)_n^-$ clusters where this has been noted.

Interestingly, for all six $(H_2O)_6^-$ isomers, the sum of the kinetic energy, electrostatic, and repulsive contributions to the Drude CI and PM3 energies is very small, with the result being that the net EBEs are roughly equal to the correlation (polarization) contributions. From Figure 17, it is seen that the polarization potential is negligible for $r \gtrsim 4$ Å (as measured from the center-of-mass of a monomer). This suggests that for large clusters it

will not be necessary to include the Drude oscillators or polarization potentials on water molecules far from the excess electron (allowing, of course, for the spatial extent of the electron distribution). To test this idea, we report in Figure 21 the EBE of the $(H_2O)_6^-$ chain (6D) with successive (starting from the end furthest from the excess electron) Drude oscillators or polarizable centers removed. From this figure, it is seen that the contribution of correlation (polarization) effects drops off rapidly along the chain with nearly the full contribution being recovered when Drude oscillators (polarization centers) are included on only the three waters on the acceptor end of the chain. It is noteworthy that nearly identical correlation contributions from the different monomers are obtained in the Drude CI and PM3 model potential approaches. This result confirms that for large clusters and for simulations of e_{aq}^- it is necessary to include Drude oscillators (or polarizable sites) on only a relatively small subset of the water monomers, thereby greatly reducing the computational cost of the calculations. The challenge, of course, is to determine, through some sort of prescreening procedure, an estimate of the charge distribution of the excess electron, for use in deciding on which water monomers to include Drude oscillators or polarizable sites. There are several ways that one could envision accomplishing this. For example, one could use a small DVR in the prescreening calculations.

For the four $(H_2O)_6$ isomers with large dipole moments, the Drude model CI and PM3 models give EBEs that agree to within 4%. However for 6E and 6F, with zero dipole moments and "cavity-bound" anion states, the PM3 values of the EBEs are 9 and 17% larger than the Drude CI values, with the latter being in closer agreement with the *ab initio* CCSD(T) results. As will be seen below, the PM3 model consistently gives larger EBEs than the Drude model, particularly in the case of cavity-bound anions.

For the six $(H_2O)_6^-$ clusters the EBEs from the TB polarization model are in poorer agreement with the *ab initio* CCSD(T) results than are the EBEs from the Drude model CI or the PM3 polarization model calculations, with the average absolute difference between the TB and CCSD(T) EBEs being 30%. With the exception of 6E, the TB model gives smaller EBEs than do the Drude model or *ab initio* CCSD(T) calculations. Examination of the individual contributions to the EBEs in Table I provides an explanation of this behavior. For all six $(H_2O)_6^-$ isomers, the polarization contribution to the energy is appreciably

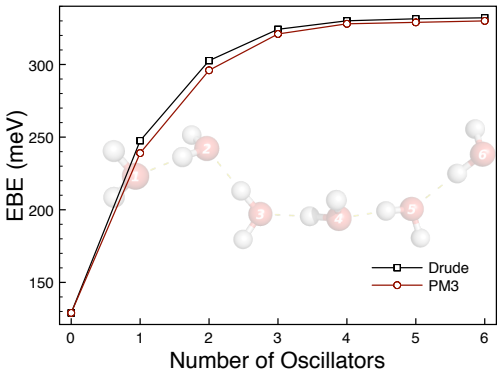

Figure 21: Hexamer isomer 6E with incremental inclusion of Drude oscillators. Zero indicates that each water only contributes to the ES+rep potential. Points 1-6 have incrementally included those oscillators in the CI step. The black line is the Drude model CI and the red line is the PM3 polarization potential.

smaller in the TB model than in the Drude and PM3 models. (Here we have equated the correlation corrections in the Drude model with the polarization contributions in the polarization models.) With the exception of 6E, the electrostatic contributions to the total energy are roughly the same in the three models. On the other hand, for 6E, in which there are six OH groups, relatively close together, pointed toward the cavity center, the electrostatic contribution is about eight times larger in the TB model than in the Drude or PM3 models, which more than compensates for the weak polarization in the TB approach. For the other five isomers, the enhanced electrostatic interactions in the TB model do not compensate for the underestimation of the polarization contribution.

4.4 RESULTS FOR $(H_2O)^-_{20}$ AND $(H_2O)^-_{24}$

The six $(H_2O)^-_{20}$ clusters considered in this work and depicted in Fig. 22 all have dodecahedral structures that differ in the orientations of the OH groups, with dipole moments that range from 0 to 25 D. The five $(H_2O)^-_{24}$ clusters in figure 23, on the other hand, all have zero

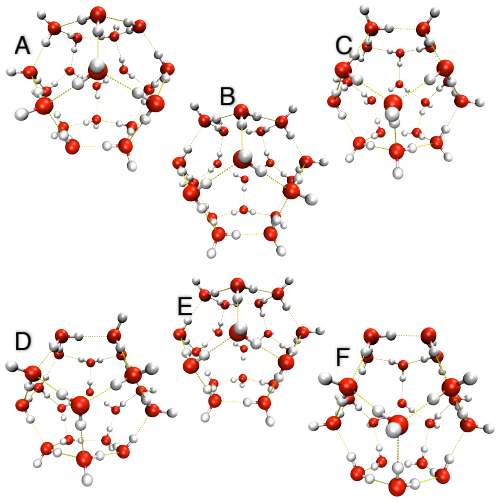

Figure 22: Six $(H_2O)_{20}^-$ isomers from Herbert and Head-Gordon[93, 94]. All isomers are rearrangements of hydrogens in a 5^{12} cage.

dipole moments. These $(H_2O)_{20}^-$ and $(H_2O)_{24}^-$ structures were "built" by Herbert and Head-Gordon,[93, 94] and are expected to be appreciably less stable than the global potential energy minima. All six $(H_2O)_{20}^-$ clusters and two of the $(H_2O)_{24}^-$ clusters (24B, and 24E) have surface bound excess electron states. The other three $(H_2O)_{24}^-$ clusters have cavity-bound excess electron states.

For the four $(H_2O)_{20}$ clusters with large dipole moments, the EBE's obtained from the Drude model CI and PM3 approaches are in excellent agreement with each other and with the *ab initio* MP2 results of Herbert and Head-Gordon. However, for the $(H_2O)_{20}$ and $(H_2O)_{24}$ clusters with zero or near zero dipole moments, the situation is quite different. For these clusters, the Drude model CI and PM3 approaches give much larger EBEs than obtained from the MP2 calculations. (In fact, for 24C, the MP2 calculations fail to bind the excess electron, and for 24D and 24C they bind the excess electron only weakly.) The large differences between the model potential and *ab initio* MP2 EBEs for these species is largely a consequence of inadequacy of the Hartree-Fock reference wavefunctions rather than a deficiency of the Drude model or polarization model approaches. The inadequacy of the MP2 calculations for this group of clusters stems from the failure of the Hartree-Fock method

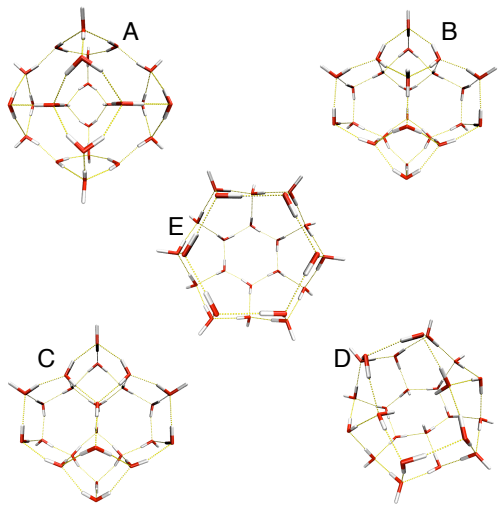

Figure 23: Five $(H_2O)_{24}^-$ isomers from Herbert and Head-Gordon[93, 94].

to provide a suitable zeroth-order wavefunction. Indeed, the Hartree-Fock calculations either fail to bind the excess electron or bind it only very weakly (with the exception of 24D).

Herbert and Head-Gordon devised an interesting strategy, referred to here as s-MP2(BHLYP), for dealing with the situation that the Hartree-Fock approximation fails to bind or only weakly binds the excess electron.[94] In this approach the EBEs are calculated using the MP2 method, but with BHLYP[139] orbitals and orbital energies in place of the corresponding Hartree-Fock quantities, together with the application of a scaling factor. The success of the s-MP2(BHLYP) method stems from the fact that the BHLYP procedure binds the excess electron even in those cases where the Hartree-Fock method does not. For the seven $(H_2O)_{20}^-$ and $(H_2O)_{24}^-$ clusters with zero or near-zero dipole moments, the EBEs calculated with the s-MP2(BHLYP) procedure are in reasonable agreement with the Drude model CI results, with the average absolute difference, excluding 20F and 24B species, which bind the excess electron only weakly even in the Drude CI approach, being 21%. For the $(H_2O)_{20}$ clusters with large dipole moments, the MP2 and s-MP2(BHLYP) procedures give nearly the same EBEs, which, in turn, are close to the Drude model results.

Although the s-MP2(BHLYP) method solves the major problem associated with MP2 calculations for $(H_2O)_n^-$ clusters for which the Hartree-Fock method does not provide a

suitable zeroth-order wavefunction, it is likely that the Drude model CI approach provides more accurate estimates of the EBEs for these clusters. There is a need for high quality *ab initio* calculations of the EBEs for clusters such as 20E, 20F, and 24A-24E to determine whether this is indeed the case. Such calculations will be very challenging since they will require an approach such as EOM-CC that does not require the excess electron to be bound in the Hartree-Fock approximation, together with the use of large, flexible basis sets. For the $(H_2O)_{20}$ and $(H_2O)_{24}$ clusters with zero or near-zero dipole moment the PM3 approach gives larger (by up to 50%) EBEs than obtained with the Drude model CI approach, whereas for the clusters with large dipole moments these two approaches give similar values for the EBEs. As noted above, for 6E and 6F, which also have zero dipole moments, the PM3 method overestimates the EBEs by about 11%. The reason for the greater disparity between the Drude model and PM3 values of the EBEs for these larger clusters is not clear. However, it should be recalled that the damping parameters in the two models were chosen so that the model potentials reproduce the CCSD(T) value of the EBE of $(H_2O)_2^-$. $(H_2O)_2^-$ is a dipole-bound anion, with an EBE of only about 40 meV and a much more extended charge distribution than for the cavity-bound anions of $(H_2O)_{20}$ and $(H_2O)_{24}$.

Based on the results for 6E and 6F, we anticipate that, in general, the Drude model provides more accurate estimates of the EBEs than does the PM3 polarization model. Again, calculations using a method such as EOM-CC would be required to establish this. We note also that the overall agreement between the EBEs calculated using the PM3 and the Drude models for the entire set of clusters considered can be improved by more strongly damping the polarization term in the PM3 model.

For all ten $(H_2O)_{20}^-$ and $(H_2O)_{24}^-$ clusters the TB model gives appreciably smaller EBEs than obtained from Drude model CI calculations. The ratio of the EBEs from the Drude model CI and TB methods ranges from 1.4 to 1.6 for the clusters with large dipole moments and from 1.6 to 4.0 D for the clusters with zero or near zero dipole moments, excluding 24C, for which the ratio is 21. As discussed above for the $(H_2O)_6^-$ isomers, the weaker the electron binding in the TB model is a consequence of its weak polarization potential.

4.5 $(H_2O)_{45}^-$ CLUSTERS

The two $(H_2O)_{45}^-$ clusters chosen for study are low-energy species identified in molecular dynamics simulations of Turi and Rossky.[105] As seen from Fig 24, the excess electron is localized in the interior of the cluster in 45A and is surface bound in 45B. For $(H_2O)_{45}^-$ there are no *ab initio* results with which to compare. Both $(H_2O)_{45}^-$ isomers bind the excess electron by about 700 meV in the ES+rep approximation. For 45A the EBEs calculated from the Drude model CI, PM3, and TB calculations are 2508, 2861 and 2356 meV, respectively, while for 45B, the corresponding EBEs are 1350, 1480, and 986 meV. Thus, electron correlation effects contribute over 1 eV more to the EBE of 45 A than that of 45B, consistent with there being many more water monomers "close" to the excess electron in 45A than in 45B.

In the Drude CI calculations the radius of gyration of the excess electron is 2.2 and 3.5 Å, for 45A and 45B, respectively. Interestingly, the radius of gyration calculated for the cavity-bound anion 45A is close to that of e_{aq}^-. For 45A and 45B, the EBE calculated using the PM3 model is only about 10% larger than that calculated using the Drude CI approach. In contrast, the TB approach gives smaller EBEs than does the Drude model CI method, with the differences being 6 and 29% for 45A and 45B, respectively. 45A, like 6E discussed above, has multiple OH groups pointing toward the excess electron which causes a large overestimation of the electrostatic contribution to the EBE in the TB model which partially compensates for the underestimation of the polarization contribution in this approach. 45A is unique among the clusters considered in that the second-order induction correction in the Drude model approach is larger than the second-order dispersion correction to the EBE.

4.6 RELIABILITY OF MODEL POTENTIAL APPROACHES FOR PREDICTING RELATIVE ENERGIES OF $(H_2O)_N^-$ ISOMERS

Although the focus of this article has been on the use of model potential approaches for EBEs of $(H_2O)_n^-$ clusters, equally important is the use of model potential approaches for predicting the relative stability of different isomers of these clusters. This requires that the model

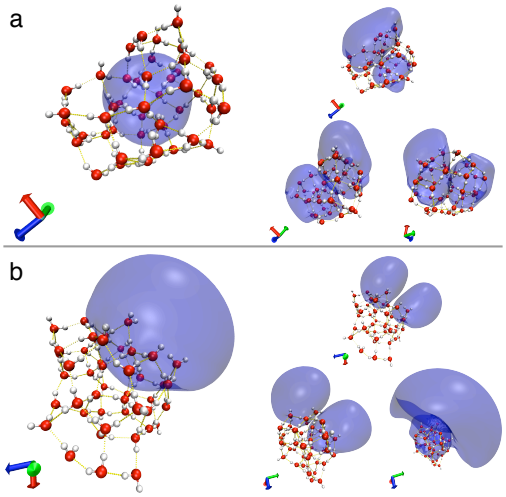

Figure 24: Two isomers of $(H_2O)_{45}^-$ from finite temperature simulations.[105] (a) 90% density of the ground state for the interior anion (45A). Top-left 90% density of first excited state. Bottom-left, 90% density of the second excited state. Bottom-right 80% density of the third excited state. (b) 90% density of the ground state for the surface anion (45B). Top-left 90% density of first excited state. Bottom-left, 90% density of the second excited state. Bottom-right 75% density of the third excited state.

Table 10: Relative energies (meV) of the six $(H_2O)_6^-$ isomers.

	6A		6B		6C		6D		6E		6F	
	Neutral	Anion	Neutral	Anion	Neutral	Anion	Neutral	Anion	Neutral	Anion	Neutral	Anion
DPP	0.00	0.00	290	172	−27	50	265	384	604	490	1814	1430
SPC	0.00	0.00	442	259	−48	7	109	252	908	605	2213	2139
MP2	0.00	0.00	293	153	−102	22	273	343	557	467	1841	1497
CCSD(T)	0.00	0.00	293	153	−111	19	293	383	549	469	1824	1518

potential approach be able to accurately predict both the EBEs and the relative energies of the neutral clusters. Most model potential studies of $(H_2O)_n^-$ clusters have employed non-polarizable SPC[140] or SPC/E[72] force fields, which are known to fare poorly in describing the energetics of neutral water clusters.[141, 142] This can be seen from Table 10 which compares the relative energies of the neutral 6A and 6F clusters, at the anion geometries, calculated using the *ab initio* CCSD(T)/aug-cc-pVTZ[143] method and with the SPC and DPP water models, which are used in the TB and Drude (and PM3) models, respectively. It is seen from this table that the DPP water model is more successful at reproducing the relative energies of the neutral clusters than is the SPC model, with the average errors (determined by comparison with the CCSD(T) results being −0.46 and −3.6 kcal/mol with the DPP and SPC models, respectively. In our earlier versions of the quantum Drude model we adopted the polarizable Dang-Chang model[26] for the water force field. Although the Dang-Change model has proven successful for describing water in a range of environments, we have found that it does not do a good job at describing the relative energies of the neutral clusters at the geometries adopted in the anions.[19] Indeed, this is what motivated us to develop the DPP model, which fares much better in this regard.

Table 10 includes the relative energies of the anions of 6A-6F calculated using the various theoretical methods. As expected, the Drude/DPP approach gives relative energies close to the CCSD(T) results, while the TB/SPC method gives relative energies appreciably different from the CCSD(T) results. As seen from Table 9, in spite of the overall success of the Drude/DPP approach at predicting the relative energies of the different $(H_2O)_6^-$ isomers, there are differences as large as 2 kcal/mol, with most of the differences being associated with the neutral clusters.

Table 11: Ground and bound excited state energies (meV) from Drude/DPP CI and PM3 local potential for $(H_2O)_{13}^-$ and $(H_2O)_{45}^-$ isomers.

	13			45A			45B		
	CI	PM3	TB	CI	PM3	TB	CI	PM3	TB
Ground	1119	1173	807	2508	2861	2606	1395	1480	1103
1st	182	229	106	554	762	272	599	643	374
2nd	52	68	29	471	730	192	491	572	338
3rd	—	2	—	450	709	94	205	322	135

4.7 EXCITED STATES

Experimentally, it has been found that for the $(H_2O)_n^-$, $n < 32$ ions, vertical excitation of the excess electron leads to direct photodetachment to the continuum, whereas for the $32 < n < 64$ clusters, vertical excitation assesses bound (with respect to electron detachment) excited states.[144] Both the Drude model CI and the polarization model approaches are able to describe these excited states of $(H_2O)_n^-$ clusters, although the lack of *ab initio* data on the excited states prevents us from assessing the accuracy of the model potential approaches for characterizing the excited states. However, given the fact that the excited state wavefunctions are much more spatially extended than the ground state wavefunctions, it is reasonable to expect that the Drude and PM3 model potential approaches perform even better for the excited states than for the ground states.

Although the geometrical structures of the observed $(H_2O)_n^-$, $n > 8$, ions are unknown, there is evidence that the dominant species have an AA electron binding site (at least in the $n = 11 - 13$ clusters).[145] For this reason, in comparing the various model potential approaches for describing the excited states of $(H_2O)_n^-$, we include a low-energy isomer of $(H_2O)_{13}^-$ with an AA binding site (Figure 25). We also report excitation energies and charge distributions for 45A and 45B, which are representative of surface and interior bound species

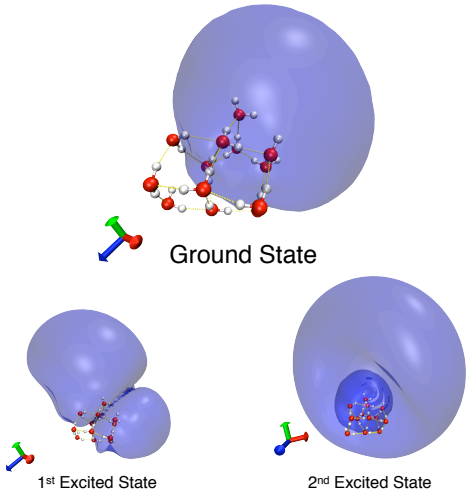

Figure 25: Ground and the two bound excited states of $(H_2O)_{13}^-$.

in the large cluster regime. Table 11 reports the excitation energies of these three clusters calculated using the Drude model CI, PM3, and TB approaches. The charge distributions for the ground and lowest energy excited states as described by the Drude CI approach for the three clusters are shown in Figs. 24 and 25.

For all three clusters the charge distribution of the ground state is approximately s-like and the charge distributions of the three low-lying excited states are p-like. Thus the electronic transitions can be qualitatively described as $s \rightarrow p$ independent of whether the excess electron is cavity- or surface-bound. This conclusion was also reached by Turi and Rossky in their recent study of $(H_2O)_n^-$ clusters.[104]

For the three clusters considered, the Drude and PM3 models give similar excitation energies, whereas the excitation energies from the TB model differ by up to 20% from the corresponding Drude model CI results. For the $(H_2O)_{13}^-$ cluster chosen for study, the calculated excitation energies (937 and 1067 meV) are in good agreement with experiment, for which the peak in the absorption spectrum occurs near 1100 meV.[88]

4.8 SUMMARY

It is well known from *ab initio* electronic structure calculations that electron correlation effects play a major role in the binding of excess electrons to water clusters and clusters of other polar molecules. Interestingly, these correlation effects can be accurately modeled by use of quantum Drude oscillators in which the ten electrons on each water monomer are modeled by a 3-dimensional Drude oscillator. By use of an adiabatic separation between the excess electron and the Drude oscillators, it is possible to derive a polarization potential model for the excess electron. This clearly demonstrates that one-electron models with polarization terms are able to recover the correlation interactions between the excess electron and the more tightly bound electrons of the monomers. For most clusters considered, the polarization potential approach gives electron binding energies in close agreement with the Drude model results, although for clusters with cavity-bound excess electron states, the EBEs from the polarization potential approach tend to be somewhat larger that the Drude model results.

Ab initio Hartree-Fock calculations do not provide a proper zeroth-order wavefunction of several of the clusters with zero or near zero dipole moments. Both the Drude model, when used in conjunction with the CI method, and the polarization model approaches provide realistic descriptions of the anion states for these challenging systems.

It has also been demonstrated that correlation (polarization) contributions from water molecules more than ~ 4 Å from from the excess electron are unimportant, although, to exploit this computationally it will first be necessary to obtain a rough estimate of the distribution of the excess electron (perhaps using preliminary calculations with smaller basis sets). Such strategies will enable accurate calculations on the anion states of $(H_2O)_n$ clusters containing hundreds of monomers.

Both, the Drude and PM3 polarization models, in their present implementations, are not fully self consistent, in that the interaction between the excess electron and one of the monomers does not alter the interaction with the other monomers. The model Hamiltonians can be readily modified to allow for such many-body interactions. Given the magnitude of the correlation contributions to the EBEs, it is surprising that the Drude and PM3 models,

which neglect these interactions fare as well as they do.

We also showed that to accurately describe the relative energies of the various isomers of a $(H_2O)_n^-$ cluster, it is essential that one employ a realistic model for the electron-water interactions as well as one that provides an accurate description of the neutral water clusters. Our work indicates that many common water models do not meet this requirement.

In concluding, we note that one of the major challenges in modern electronic structure theory is the development of methods for treating long-range inter- and intra-molecular correlation effects. Some of the most promising such methods involve separating the r_{ij}^{-1} operator into short-range and long-range parts, which are then treated by different theoretical methods, e.g., treating short-range correlation via DFT and long-range correlation using MP2.[146] Although our work has focused on excess electrons interacting with water clusters, it does suggest that it may be possible to employ Drude oscillators or polarization potential approaches for treating long-range correlation effects in other systems. Indeed, there are some similarities between our Drude-model approach and Johnson and Becke's exchange-hole approach for treating intermolecular dispersion.[147]

5.0 PARALLEL TEMPERING MONTE CARLO SIMULATIONS OF THE WATER HEPTAMER ANION

This work has been published as Ref. [60]

5.1 INTRODUCTION

Negatively charged water clusters have been known since their observation, mass spectroscopically, by Haberland *et al.* in 1984.[106, 148] However, only recently, with the application of vibrational predissociation spectroscopy, has a clear picture of the geometrical structures of small $(H_2O)_n^-$ clusters emerged.[149, 150, 151, 152, 97, 153, 99, 98, 145, 103, 100, 61] $(H_2O)_7^-$ is particularly intriguing in that the recent predissociation studies of Roscioli and co-workers have revealed the existence of at least four isomers, three with high electron binding energies (EBE) and containing a double acceptor (AA) monomer and one with low EBE and lacking an AA monomer.[61] In the present study Monte Carlo[154] simulations are used together with the quantum Drude model[155, 128, 129, 62] to characterize the $(H_2O)_7^-$ cluster at finite temperatures. Configurations sampled at $T = 200$, 142, and 100 K are quenched to local minima to provide insight into the types of structures that are present under equilibrium conditions.

5.2 COMPUTATIONAL DETAILS

In carrying out simulations of negatively charged water clusters, it is crucial to employ a theoretical method that accurately describes both the water-water and the electron-water interactions.[63, 109, 108] In principle, this could be accomplished using *ab initio* electronic structure methods; but to achieve the accuracy required requires the use of a large basis set and inclusion of high-order electron correlation effects, e.g., using the CCSD(T) method.[156, 157] The high computational cost of such calculations precludes their use in Monte Carlo or molecular dynamics simulations where millions of configurations need to be sampled. In this work, we circumvent this problem by using the distributed point polarizable (DPP)[19] water model to describe the water-water interactions and the quantum Drude model[155, 128, 129, 62] to describe the excess electron-water interactions. The total energy of the anion is given by the energy of the neutral water cluster minus the electron binding energy. (Here we are employing the convention that a bound anion has a positive EBE.) This model potential approach has been found to give electron binding energies and relative energies of different isomers in excellent agreement with the results of high-level *ab initio* electronic structure calculations, but because it is orders of magnitude computationally faster than *ab initio* calculations,[130] it can be used in finite temperature simulations.

The DPP and quantum Drude models have been described in detail in references [19, 155, 128, 129, 62]. Here we note that the DPP model, like the TTM2-R model,[27] employs rigid monomers, with the experimental gas-phase values of the OH bond distance and HOH angle, three point charges (0.574 $|e|$ on the H atoms and -1.148 $|e|$ on an M site, displaced 0.25 Å from O atom toward the H atoms along the HOH bisector). With these charges and their locations, the DPP model gives dipole and quadrupole moments close to the experimental values for the monomer. Each monomer has three, atom centered, polarizable sites, and mutual interaction between polarizable sites on a monomer are permitted. A Thole-type damping procedure[30] is used for charge–induced-dipole and induced-dipole–induced-dipole interactions. Damped C_6/R^6 dispersion interactions are employed between O atoms, and exponential repulsion interactions are employed between all atoms of different monomers. The Hamiltonian for the excess electron includes interactions with the point charges, the

induced-dipoles, and a short-range repulsive core associated with each monomer. The excess electron also interacts with a quantum Drude oscillator, centered on the M site on each monomer, to account for the electron-water induction and dispersion interactions. The electron binding energy is calculated through a configuration interaction method with a Gaussian basis set[62] for the excess electron and harmonic oscillator functions for each Drude oscillator.

The simulations were carried out using the parallel tempering (PTMC) algorithm,[158] which helps avoid trapping in local regions of configuration space. In the application of the PTMC method to $(H_2O)_7^-$, twelve replicas, with temperatures ranging from 42 to 200 K, were employed. Most moves within each replica are carried out with standard Metropolis sampling,[159] with every 250^{th} move involving attempted exchanges between replicas at adjacent temperatures. The Metropolis moves (translations and rotations) involved displacements of single water molecules only. The maximum step sizes and the temperature values used were chosen so that about 50% of the Metropolis and exchange moves are accepted. The simulations employed an equilibration period of three million moves, followed by a production period of four million moves (for each replica). For the $T = 100$, 142, and 200 K replicas, every thousandth configuration was saved and used for subsequent quenching to a local minimum through numerical geometry optimization using the Broyden-Fletcher-Goldfarb-Shanno (BFGS) method[160].

5.3 RESULTS

Fig. 26 reports the temperature dependence, over the $50 - 200$ K range of the EBE distributions of $(H_2O)_7^-$ obtained from the PTMC simulations. At $T = 50$ K, there is a single relatively narrow peak centered near an EBE of 240 meV. As the temperature increases, this feature broadens and moves to lower energies. At high (i.e., $T = 200$ K) temperatures, a second weak, broad peak centered near an EBE of 450 meV, also appears. It is clear from these results that there are two classes of structures, one with low ($\lesssim 300$ meV) EBEs and the other with high ($\gtrsim 400$ meV) EBEs, with the latter acquiring sizable population only

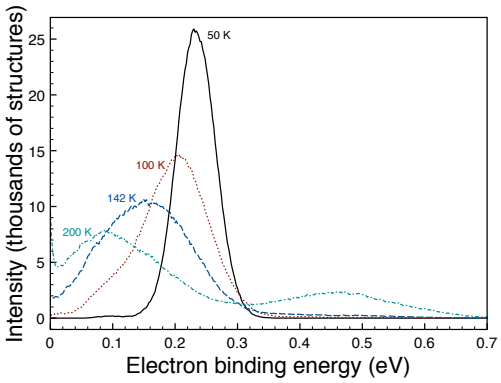

Figure 26: Electron binding energy distributions associated with the $T = 100$, 142, and 200 K replicas in the PTMC simulations of $(H_2O)_7^-$.

at high temperatures. The energies of the peaks in the EBE distributions are in excellent agreement with those in the experimental photoelectron spectra,[61, 88] although the experimental studies show a strong preference for the high EBE isomers, even in the case of the Ar-tagged clusters, for which the temperature is estimated to be ~ 50 K.

Selected low-energy forms of $(H_2O)_7^-$ obtained from the quenching calculations are illustrated in Figure 27. All of these species can be viewed as originating from insertion of a water monomer into one of the edges of cage and prism isomers of $(H_2O)_6$.[161] It is also useful to differentiate the isomers according to whether or not they contain an AA binding site.

Fig. 28 reports for $(H_2O)_7^-$, the total energies relative to that of the global minimum isomer as well as the electron binding energies of the quenched isomers. The global minimum is a prism-type non-AA species with an EBE of 246 meV. This isomer was identified in the theoretical work of Kim *et al.*[91] who denoted it "PRB." (The energy of the PRB isomer appears to have been incorrectly reported in Ref. [91], and as a result it was not recognized as the global minimum in that work.) The quenching calculations locate a total of 35 isomers energetically below the most stable AA isomer, PNFA, which was also identified in Ref. [91] and which is predicted in the present study to be 61 meV above the global minimum. Most of these low-energy structures, are prism-like and were not reported in an earlier theoretical

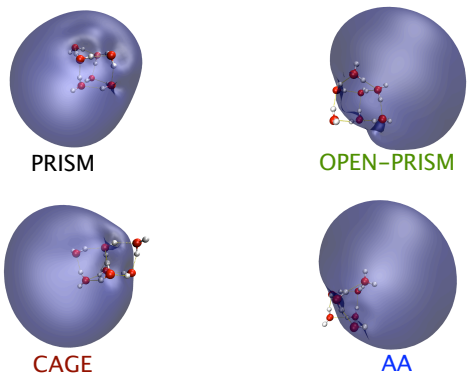

Figure 27: Structural motifs sampled in the PTMC simulations of $(H_2O)_7^-$. The non-AA species are labeled as prism, open-prism, and cage, drawing on their resemblance to low-energy isomers of $(H_2O)_6$. The color codes match those in later figures.

studies of $(H_2O)_7^-$.[91, 162] With one exception, all isomers below the most stable AA species have low ($\lesssim$ 250 meV) EBE's. The exception is isomer H-b, which is calculated to lie 56 meV above the global minimum, with an EBE of 445 meV. This isomer is shown in Fig. 29 together with other selected low-energy isomers, including the global minimum. Figure 30 reports the EBEs *vs.* the dipole moments of the neutral clusters associated with the anionic isomers obtained by quenching the configurations sampled in the $T = 200$ K replica. Overall there is a strong correlation between the EBE and dipole moment independent of whether or not the cluster contains an AA site.

As is apparent from Figs. 28(c) and 31, the $T = 200$ K replica includes a large number of AA isomers with high (up to 790 meV) EBE's. Many of these have "branched structures", some of which are depicted in Fig. 31. Presumably, the barriers for rearranging these "open" isomers to the more stable, more "compact" isomers, are relatively low. In that case, the branched isomers, if formed experimentally, would be expected to be "annealed out" in the supersonic jet expansion. We note also, that the AA isomers from the quenching calculations can be divided into two groups, one with EBEs near 440 meV and the other with EBEs near 560 meV. This is most apparent from the quenching of the structures sampled at $T = 142$ K (Fig. 28(b)). This is consistent with the recent experimental results of Ref. [61] where

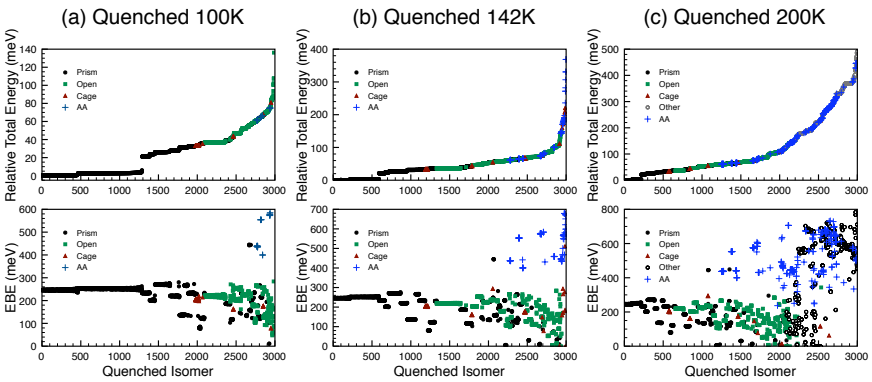

Figure 28: Relative total energies and electron binding energies of quenched structures from the T = (a) 100, (b) 142, and (c) 200 K replicas in the PTMC simulations of $(H_2O)_7^-$. AA isomers are labeled with pluses (blue), cages as triangles (red), open structures as squares (green), and prisms as circles (black). Open circles (black) in (c) correspond to isomers which have structures that differ from the motifs shown in Fig. 27. The isomers have been ordered according to total energy, relative to that of the global minimum anion, PRB.

it was found that in addition to the AA species with an EBE near 450 meV, under certain conditions a second AA species with an EBE near 600 meV is observed.

5.4 CONCLUSIONS

PTMC simulations using the quantum Drude model have been performed to calculate the electron binding energies and to enumerate low-energy isomers of $(H_2O)_7^-$. The PTMC simulations indicate that even at temperatures as high as 200 K, the equilibrium distribution of $(H_2O)_7^-$ is dominated by non-AA structures with low ($\lesssim$ 300 meV) electron binding energies, with the fraction of high ($\gtrsim$ 400 meV) EBE species, growing with increasing temperature. A total of 35 isomers are found below the most stable AA isomer, which was previously reported by Kim and co-workers[91] to be the global minimum. The high EBE species are dominated by AA clusters, although there is a small contribution from a non-AA isomer,

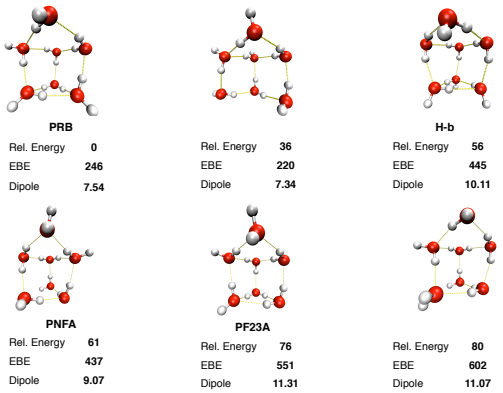

Figure 29: Selected low-energy isomers of $(H_2O)_7^-$. Also reported are the relative energies and EBEs both in meV, and the dipole moments in Debye of the associated neutral clusters. The PRB, PNFA, and PF23A isomers were reported previously in Ref. [91].

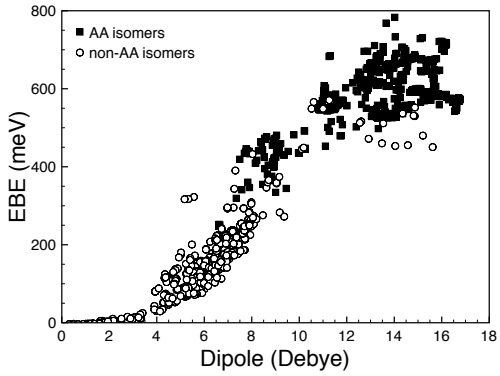

Figure 30: Electron binding energy (EBE) versus dipole moment for quenched isomers from the $T = 200$ K replica in the PTMC simulation of $(H_2O)_7^-$. AA isomers are labeled as filled squares and non-AA isomers are isomers are labeled with open circles.

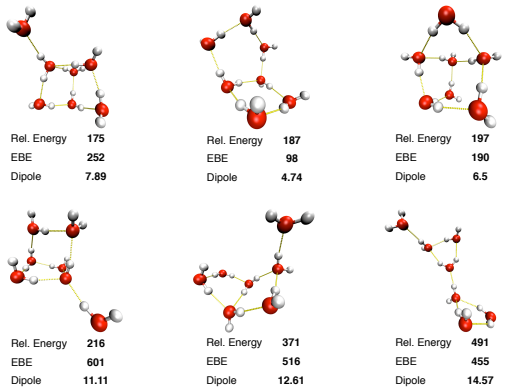

Figure 31: Representative high energy structures from quenching configurations sampled in the $T = 200$ K replica from the PTMC simulations. Total energies (meV) relative to PRB, EBEs (meV), and dipole moments (Debye) of the associated neutral clusters are reported.

with an EBE of 450 meV (H-b in Figure 29).

The energies of the peaks in the calculated EBE distributions are in close agreement with those in the measured photoelectron spectrum. However, although the low EBE species dominate the simulations, AA isomers with high EBEs dominate the experiments even in the case of Ar-tagged clusters, which have temperatures around 50 K. A similar disparity between theory and experiment has been noted for $(H_2O)_6^-$.[63] Comparison of the DPP/Drude model results with those from the large-basis set MP2 calculations reveals that the model potential approach displays a small $(20-40$ meV) bias toward the low EBE isomers.[63, 163] However, this bias is relatively small, and this does not alter our main conclusion that an equilibrium distribution of $(H_2O)_7^-$ should possess a significant population of non-AA isomers. We conclude, therefore, that the experimental formation process, for some reason, selects out the high EBE isomers. It may be that the low EBE isomers are actually formed in high yield but that most of these species are destroyed, possibly through collisions with Ar atoms before they can be detected. It is believed that in the experiments of Johnson and co-workers, most of the $(H_2O)_7^-Ar_m$ observed ions result from electron attachment to $(H_2O)_7Ar_n$ clusters, where $n > m$. Even with the attached Ar atoms, the internal energies of the neutral clusters should be on the order of $50 - 100$ meV, which means that a large

number of different forms of $(H_2O)_7^-$ would be accessible upon attachment of low-energy electrons.

6.0 SUMMARY

The Drude model introduced by Wang *et al.*[164, 128, 129, 62, 63, 130, 120] has been under steady development for five years with many recent advances. Firstly, it was discovered that employing the Dang-Chang water model[26] lead to incorrect sampling in parallel tempering simulations.[63] This prompted the development of the distributed point polarizable water model (DPP).[19] Using state-of-the-art *ab initio* packages, important contributions to the intermolecular interaction energy in water have been identified, which were used fit the DPP potential. The DPP model has been shown to reproduce relative energies of water cluster isomers with high accuracy compared to high-level *ab initio* calculations. The new Drude/DPP model recovers the accuracy of large-basis CCSD(T) calculations for several $(H_2O)_6^-$ isomers. Even though high-level *ab initio* calculations have not been performed for larger clusters, we are confident that the same accuracy is maintained.

An adiabatic approximation to the Drude/DPP model has been developed whereby the quantum harmonic oscillators on each water molecule are replaced with a potential to mimic the water response. As shown above, in the limit of large separation between the water cluster and the electron, the leading term of the adiabatic potential is similar to $\alpha/2r^4$ polarization potentials which have been extensively employed in literature for electron molecule interactions.[136, 137, 138] Our work has shown that these polarization potentials can recover some of the dispersion interactions present in our Drude/DPP model. The computational effort of the polarization potentials approach is appreciably faster than the full quantum Drude/DPP calculations. This will allow us to study much larger clusters and perform molecular dynamics simulations.

Recent experiments from Johnson and co-workers[165] have probed water rearrangements in jet-expansions of water cluster anions. This raises questions concerning the mechanism

by which an electron can become trapped by a water cluster. For the water heptamer, geometries of neutral and anionic isomers differ by rotation of several water molecules. With the recent inclusion of analytic gradients by Choi,[166] the Drude/DPP model can be used to find low-energy pathways for electron trapping by neutral clusters.

While the bulk hydrated electron is a cavity state, small water clusters bind the excess electron in a surface state. An important question in the study of water cluster anions is when does a cluster become bulk-like with the electron occupying a cavity in the water cluster. While low dipole clusters as small as the tetramer can be built with a stable cavity state, these clusters are typically very high in total energy and are not expected to be largely populated in equilibrium ensembles, and it has been shown that very large clusters ($n = 500$) can still bind an electron on the surface.[105] Further, liquid/vapor interface simulations have shown that starting from a surface state, relaxation to a cavity state is highly sensitive to temperature.[167] The challenge in determining when a cluster becomes bulk-like may be answered by its relaxation dynamics rather than its electron binding motif.

BIBLIOGRAPHY

[1] Boys, S. F.; Bernardi, F. *Mol. Phys.* **1970,** *19,* 553 - 566.

[2] Jeziorski, B.; Moszynski, R.; Szalewicz, K. *Chem. Rev.* **1994,** *94,* 1887.

[3] Chalasinski, G.; Szczesniak, M. *Chem. Rev.* **2000,** *100,* 4227-4252.

[4] Stone, A. J. *The Theory of Intermolecular Forces;* Clarendon Press Oxford: 1996.

[5] Unsöld, *Z. Physik.* **1927,** *43,* 563-574.

[6] London, F. *Z. Physik. Chem. B* **1930,** *11,* 222-251.

[7] Casimir, H. B. G.; Polder, D. *Phys. Rev.* **1948,** *73,* 360.

[8] Murrell, J. N.; Teixeira-Dias, J. J. C. *Mol. Phys.* **1970,** *19,* 521 - 531.

[9] Soderhjelm, P.; Karlstrom, G.; Ryde, U. *J. Chem. Phys.* **2006,** *124,* 244101.

[10] Hess, O.; Caffarel, M.; Huiszoon, C.; Claverie, P. *J. Chem. Phys.* **1990,** *92,* 6049-6060.

[11] Rybak, S.; Jeziorski, B.; Szalewicz, K. *J. Chem. Phys.* **1991,** *95,* 6576.

[12] DeFusco, A.; Jenness, G.; Jordan, K. D. Unpublished data.

[13] Freitag, M. A.; Gordon, M. S.; Jensen, J. H.; Stevens, W. J. *J. Chem. Phys.* **2000,** *112,* 7300-7306.

[14] Trainor, L. E. H. *Phys. Rev.* **1954,** *95,* 801–810.

[15] Wormer, P. E. S.; Hettema, H. *J. Chem. Phys.* **1992,** *97,* 5592-5606.

[16] Elrod, M. J.; Saykally, R. J. *Chem. Rev.* **1994,** *94,* 1975-1997.

[17] Mas, E. M.; Bukowski, R.; Szalewicz, K. *J. Chem. Phys.* **2003,** *118,* 4386-4403.

[18] Mas, E. M.; Bukowski, R.; Szalewicz, K. *J. Chem. Phys.* **2003,** *118,* 4404-4413.

[19] DeFusco, A.; Schofield, D. P.; Jordan, K. D. *Mol. Phys.* **2007,** *105,* 2681 - 2696.

[20] Yu, H.; van Gunsteren, W. F. *Comput. Phys. Commun.* **2005,** *172,* 69–85.

[21] Morita, A. *J. Comput. Chem.* **2002,** *23,* 1466-1471.

[22] Lamoureux, G.; Harder, E.; Vorobyov, I. V.; Roux, B.; Alexander D. MacKerell, J. *Chem. Phys. Lett.* **2006,** *418,* 245-249.

[23] Chen, B.; Xing, J.; Siepmann, J. *J. Phys. Chem. B* **2000,** *104,* 2391-2401.

[24] Paricaud, P.; Predota, M.; Chialvo, A. A.; Cummings, P. T. *J. Chem. Phys.* **2005,** *122,* 244511.

[25] Cui, J.; Liu, H.; Jordan, K. *J. Phys. Chem. B* **2006,** *110,* 18872-18878.

[26] Dang, L. X.; Chang, T. M. *J. Chem. Phys.* **1997,** *106,* 8149.

[27] Burnham, C. J.; Xantheas, S. S. *J. Chem. Phys.* **2002,** *116,* 1500-1510.

[28] Ren, P.; Ponder, J. W. *J. Phys. Chem. B* **2003,** *107,* 5933.

[29] Fanourgakis, G.; Xantheas, S. *J. Phys. Chem. A* **2006,** *110,* 4100-4106.

[30] Thole, B. T. *Chem. Phys.* **1981,** *59,* 341–350.

[31] Halgren, T. A. *J. Am. Chem. Soc.* **1992,** *114,* 7827.

[32] Hwang, R.; Huh, S. B.; Lee, J. S. *Mol. Phys.* **2003,** *101,* 1429 - 1441.

[33] Tschumper, G. S.; Leininger, M. L.; Hoffman, B. C.; Valeev, E. F.; III, H. F. S.; Quack, M. *J. Chem. Phys.* **2002,** *116,* 690-701.

[34] Peterson, K. A.; Woon, D. E.; Thom H. Dunning, J. *J. Chem. Phys.* **1994,** *100,* 7410-7415.

[35] Xantheas, S. S.; Burnham, C. J.; Harrison, R. J. *J. Chem. Phys.* **2002,** *116,* 1493-1499.

[36] Lagutschenkov, A.; Fanourgakis, G. S.; Niedner-Schatteburg, G.; Xantheas, S. S. *J. Chem. Phys.* **2005,** *122,* 194310.

[37] Xantheas, S. S. *J. Chem. Phys.* **1995,** *102,* 4505-4517.

[38] Xantheas, S. S. *J. Chem. Phys.* **1994,** *100,* 7523-7534.

[39] Xantheas, S. S.; Thom H. Dunning, J. *J. Chem. Phys.* **1993,** *99,* 8774-8792.

[40] Brooks, B. R. "Algorithms for Molecular Dynamics at Constant Temperature and Pressure", Technical Report, DCRT Report, NIH, 1988.

[41] Andersen, H. C. *J. Comp. Phys.* **1983,** *52,* 24-34.

[42] Berendsen, H. J. C.; Postma, J. P. M.; van Gunsteren, W. F.; DiNola, A.; Haak, J. R. *J. Chem. Phys.* **1984,** *81,* 3684-3690.

[43] Allen, M. P.; Tildesley, D. J. *Computer Simulation of Liquids;* Clarendon Press: Oxford, 1987.

[44] Frisch, M. J. *et al.* "Gaussian 03, Revision D.01", 2004.

[45] Ponder, J. W. *Software Tools for Molecular Design;* Washington University School of Medicine: Saint Lous, MO, 3.9 ed.; 2001.

[46] Jenness, G.; DeFusco, A.; Cui, J.; Jordan, K. D. Unpublished data.

[47] Mas, E. M.; Szalewicz, K.; Bukowski, R.; Jeziorski, B. *J. Chem. Phys.* **1997,** *107,* 4207.

[48] Kendall, R. A.; Thom H. Dunning, J.; Harrison, R. J. *J. Chem. Phys.* **1992,** *96,* 6796.

[49] Dunning, T. H. *J. Chem. Phys.* **1989,** *90,* 1007.

[50] Pople, J. A.; Head-Gordon, M.; Raghavachari, K. *J. Chem. Phys.* **1987,** *87,* 5968-5975.

[51] Dyke, T. R.; Muenter, J. S. *J. Chem. Phys.* **1973,** *59,* 3125.

[52] Verhoeven, J.; Dymanus, A. *J. Chem. Phys.* **1970,** *52,* 3222.

[53] Murphy, W. F. *J. Chem. Phys.* **1977,** *67,* 5877-5882.

[54] Stone, A. J.; Alderton, M. *Mol. Phys.* **1985,** *56,* 1047.

[55] Stevens, W. J.; Fink, W. H. *Chem. Phys. Lett.* **1987,** *139,* 15–22.

[56] Stone, A. J. *Chem. Phys. Lett.* **1993,** *211,* 101–109.

[57] Li, H.; Gordon, M. S.; Jensen, J. H. *J. Chem. Phys.* **2006,** *124,* 214108.

[58] Tang, K. T.; Toennies, J. P. *J. Chem. Phys.* **1984,** *80,* 3726-3741.

[59] Smith, B. J.; Swanton, D. J.; Pople, J. A.; III, H. F. S.; Radom, L. *J. Chem. Phys.* **1990,** *92,* 1240-1247.

[60] DeFusco, A.; Sommerfeld, T.; Jordan, K. D. *Chem. Phys. Lett.* **2008,** *455,* 135–138.

[61] Roscioli, J. R.; Hammer, N. I.; Johnson, M. A.; Diri, K.; Jordan, K. D. *J. Chem. Phys.* **2008,** *128,* 104314.

[62] Sommerfeld, T.; Jordan, K. D. *J. Phys. Chem. A* **2005,** *109,* 11531-11538.

[63] Sommerfeld, T.; Gardner, S. D.; DeFusco, A.; Jordan, K. D. *J. Chem. Phys.* **2006,** *125,* 174301.

[64] Fanourgakis, G. S.; Apra, E.; Xantheas, S. S. *J. Chem. Phys.* **2004,** *121,* 2655-2663.

[65] Soper, A. K. *Chem. Phys.* **2000,** *258,* 121-137.

[66] Lide, D. R., Ed.; *CRC Handbook of Chemistry and Physics;* CRC press: 2003.

[67] Krynicki, K.; Green, C. D.; Sawyer, D. W. *Faraday Discuss.* **1978,** *66,* 199 - 208.

[68] Jancso, G.; Hook, W. A. V. *Chem. Rev.* **1974,** *74,* 689 - 750.

[69] Hura, G.; Sorenson, J. M.; Glaeser, R. M.; Head-Gordon, T. *J. Chem. Phys.* **2000,** *113,* 9140-9148.

[70] Pedulla, J. M.; Kim, K.; Jordan, K. D. *Chem. Phys. Lett.* **1998,** *291,* 78–84.

[71] Jorgensen, W. L.; Chandrasekhar, J.; Madura, J. D.; Impey, R. W.; Klein, M. L. *J. Chem. Phys.* **1983,** *79,* 926-935.

[72] Berendsen, H. J. C.; Grigera, J. R.; Straatsma, T. P. *J. Phys. Chem.* **1987,** *91,* 6269-6271.

[73] Bukowski, R.; Szalewicz, K.; Groenenboom, G. C.; van der Avoird, A. *Science* **2007,** *315,* 1249-1252.

[74] Garrett, B. *et al. Chem. Rev.* **2005,** *105,* 355-390.

[75] Martinez, S. E.; Huang, D.; Ponomarev, M.; Cramer, W. A.; Smith, J. L. *Protein Sci* **1996,** *5,* 1081-1092.

[76] Weyl, W. *Ann. Phys. Chem.* **1864,** *123,* 350.

[77] Hart, E. J.; Boag, J. W. *J. Am. Chem. Soc.* **1962,** *84,* 4090-4095.

[78] Mizuno, M.; Yamaguchi, S.; Tahara, T. *J. Phys. Chem. A* **2005,** *109,* 5257-5265.

[79] Silva, C.; Walhout, P. K.; Yokoyama, K.; Barbara, P. F. *Phys. Rev. Lett.* **1998,** *80,* 1086–1089.

[80] Kambhampati, P.; Son, D.; Kee, T.; Barbara, P. *J. Phys. Chem. A* **2002,** *106,* 2374-2378.

[81] Pshenichnikov, M. S.; Baltuska, A.; Wiersma, D. A. *Chem. Phys. Lett.* **2004,** *389,* 171–175.

[82] Paik, D. H.; Lee, I.-R.; Yang, D.-S.; Baskin, J. S.; Zewail, A. H. *Science* **2004,** *306,* 672-675.

[83] Turi, L.; Borgis, D. *J. Chem. Phys.* **2002,** *117,* 6186-6195.

[84] Schnitker, J.; Rossky, P. J. *J. Chem. Phys.* **1987,** *86,* 3471-3485.

[85] Rosenthal, S. J.; Schwartz, B. J.; Rossky, P. J. *Chem. Phys. Lett.* **1994,** *229,* 443–448.

[86] Borgis, D.; Rossky, P. J.; Turi, L. *J. Chem. Phys.* **2006,** *125,* 064501.

[87] Feng, D.-F.; Kevan, L. *Chem. Rev.* **1980,** *80,* 1-20.

[88] Coe, J. V.; Lee, G. H.; Eaton, J. G.; Arnold, S. T.; Sarkas, H. W.; Bowen, K. H.; Ludewigt, C.; Haberland, H.; Worsnop, D. R. *J. Chem. Phys.* **1990,** *92,* 3980-3982.

[89] Shkrob, I. *J. Phys. Chem. A* **2007,** *111,* 5223-5231.

[90] Sobolewski, A. L.; Domcke, W. *Phys. Chem. Chem. Phys.* **2002,** *4,* 4–10.

[91] Lee, H. M.; Suh, S. B.; Kim, K. S. *J. Chem. Phys.* **2003,** *118,* 9981-9986.

[92] Gutowski, M.; Skurski, P. *Recent Res. Dev. Phys. Chem.* **1999,** *3,* 245.

[93] Herbert, J.; Head-Gordon, M. *J. Phys. Chem. A* **2005,** *109,* 5217-5229.

[94] Herbert, J. M.; Head-Gordon, M. *Phys. Chem. Chem. Phys.* **2006,** *8,* 68–78.

[95] Herbert, J. M. preprints.

[96] Hammer, N.; Roscioli, J.; Johnson, M.; Myshakin, E.; Jordan, K. *J. Phys. Chem. A* **2005,** *109,* 11526-11530.

[97] Shin, J.-W.; Hammer, N. I.; Headrick, J. M.; Johnson, M. A. *Chem. Phys. Lett.* **2004,** *399,* 349–353.

[98] Hammer, N.; Roscioli, J.; Johnson, M. *J. Phys. Chem. A* **2005,** *109,* 7896-7901.

[99] Hammer, N. I.; Roscioli, J. R.; Bopp, J. C.; Headrick, J. M.; Johnson, M. A. *J. Chem. Phys.* **2005,** *123,* 244311.

[100] Roscioli, J. R.; Johnson, M. A. *J. Chem. Phys.* **2007,** *126,* 024307.

[101] Verlet, J. R. R.; Bragg, A. E.; Kammrath, A.; Cheshnovsky, O.; Neumark, D. M. *Science* **2005,** *307,* 93-96.

[102] Bragg, A.; Verlet, J.; Kammrath, A.; Cheshnovsky, O.; Neumark, D. *J. Am. Chem. Soc.* **2005,** *127,* 15283-15295.

[103] Asmis, K. R.; Santambrogio, G.; Zhou, J.; Garand, E.; Headrick, J.; Goebbert, D.; Johnson, M. A.; Neumark, D. M. *J. Chem. Phys.* **2007,** *126,* 191105.

[104] Turi, L.; Sheu, W.-S.; Rossky, P. J. *Science* **2005,** *309,* 914-917.

[105] Turi, L.; Madarasz, A.; Rossky, P. J. *J. Chem. Phys.* **2006,** *125,* 014308.

[106] Haberland, H.; Schindler, H. G.; Worsnop, D. R. *Ber. Bunsen-Ges. Phys. Chem.* **1984,** *88,* 270.

[107] Weber, J. M.; Leber, E.; Ruf, M. W.; Hotop, H. *The European Physical Journal D - Atomic, Molecular, Optical and Plasma Physics* **1999,** *7,* 587–594.

[108] Gutowski, M.; Skurski, P.; Jordan, K. D.; Simons, J. *Int. J. Quantum Chem.* **1997,** *64,* 183-191.

[109] Gutowski, M.; Skurski, P.; Boldyrev, A. I.; Simons, J.; Jordan, K. D. *Phys. Rev. A* **1996,** *54,* 1906–1909.

[110] Pople, J. A.; Head-Gordon, M.; Raghavachari, K. *J. Chem. Phys.* **1987,** *87,* 5968-5975.

[111] Gutowski, M. unpublished results.

[112] Koch, W.; Holthausen, M. C. *A Chemist's Guide to Density Functional Theory;* Wiley-VCH: 2nd ed.; 2001.

[113] Cohen, A. J.; Mori-Sánchez, P.; Yang, W. *J. Chem. Phys.* **2007,** *127,* 034101.

[114] Barnett, R. N.; Landman, U.; Cleveland, C. L.; Jortner, J. *J. Chem. Phys.* **1988,** *88,* 4429-4447.

[115] Nicolas, C.; Boutin, A.; Lévy, B.; Borgis, D. *J. Chem. Phys.* **2003,** *118,* 9689-9696.

[116] Wallqvist, A.; Martyna, G.; Berne, B. J. *J. Phys. Chem.* **1988,** *92,* 1721-1730.

[117] Benjamin, I.; Evans, D.; Nitzan, A. *J. Chem. Phys.* **1997,** *106,* 6647-6654.

[118] Turi, L.; Gaigeot, M.-P.; Levy, N.; Borgis, D. *J. Chem. Phys.* **2001,** *114,* 7805-7815.

[119] Jordan, K. D. *Accounts of Chemical Research* **1979,** *12,* 36-42.

[120] Jordan, K. D.; Wang, F. *Annual Review of Physical Chemistry* **2003,** *54,* 367-396.

[121] Simons, J.; Jordan, K. D. *Chem. Rev.* **1987,** *87,* 535-555.

[122] Wallis, R. F.; Herman, R.; Milnes, H. W. *J. Mol. Spec.* **1960,** *4,* 51–74.

[123] Crawford, O. H. *Mol. Phys.* **1971,** *20,* 585 - 591.

[124] Landau, L. D. Quantum Mechanics. In , 2 ed.; Pergamon Press: Oxford, 1959.

[125] Crawford, O. H.; Koch, B. J. D. *J. Chem. Phys.* **1974,** *60,* 4512-4519.

[126] Garrett, W. R. *J. Chem. Phys.* **1982,** *77,* 3666-3673.

[127] Born, M.; Oppenheimer, R. *Ann. Phys. (Leipzig)* **1927,** *84,* 457.

[128] Wang, F.; Jordan, K. D. *J. Chem. Phys.* **2001,** *114,* 10717-10724.

[129] Wang, F.; Jordan, K. D. *J. Chem. Phys.* **2002,** *116,* 6973-6981.

[130] Sommerfeld, T.; Jordan, K. *J. Am. Chem. Soc.* **2006,** *128,* 5828-5833.

[131] Koopmans, T. *Physica* **1934,** *1,* 104–113.

[132] Stanton, J. F.; Bartlett, R. J. *J. Chem. Phys.* **1993,** *98,* 7029-7039.

[133] Skurski, P.; Gutowski, M.; Simons, J. *Int. J. Quantum Chem.* **2000,** *80,* 1024-1038.

[134] Stanton, J. *et al.* "ACES II is a program product of the Quantum Theory Project", .

[135] Rigby, M.; Smith, E. B.; Wakeham, W. A.; Maitland, G. C. *The Forces Between Molecules;* Oxford: 1986.

[136] Petrov, I. D.; Sukhorukov, V. L.; Hotop, H. *Journal of Physics B: Atomic, Molecular and Optical Physics* **1999,** *32,*.

[137] Nicklass, A.; Stoll, H. *Mol. Phys.* **1995,** *86,* 317 - 326.

[138] Morrison, M. A.; Saha, B. C.; Gibson, T. L. *Phys. Rev. A* **1987,** *36,* 3682–3698.

[139] Rienstra-Kiracofe, J.; Tschumper, G.; Schaefer, H.; Nandi, S.; Ellison, G. *Chem. Rev.* **2002,** *102,* 231-282.

[140] Berendsen, H. J. C.; Postma, J. P. M.; van Gunsteren, W. F.; Hermans, J. *Intermolecular Forces;* Reidel: Dordrecht: 1981.

[141] James, T.; Wales, D. J.; Hernndez-Rojas, J. *Chem. Phys. Lett.* **2005,** *415,* 302–307.

[142] Kabrede, H.; Hentschke, R. *J. Phys. Chem. B* **2003,** *107,* 3914-3920.

[143] Dunning Jr, T. H. *J. Chem. Phys.* **1989,** *90,* 1007-1023.

[144] Ayotte, P.; Johnson, M. A. *J. Chem. Phys.* **1997,** *106,* 811-814.

[145] Roscioli, J.; Hammer, N.; Johnson, M. *J. Phys. Chem. A* **2006,** *110,* 7517-7520.

[146] Ángyán, J. G.; Gerber, I. C.; Savin, A.; Toulouse, J. *Phys. Rev. A* **2005,** *72,* 012510.

[147] Johnson, E. R.; Becke, A. D. *J. Chem. Phys.* **2006,** *124,* 174104.

[148] Haberland, H.; Ludewigt, C.; Schindler, H.-G.; Worsnop, D. R. *J. Chem. Phys.* **1984,** *81,* 3742-3744.

[149] Kim, J.; Becker, I.; Cheshnovsky, O.; Johnson, M. A. *Chem. Phys. Lett.* **1998,** *297,* 90–96.

[150] Ayotte, P.; Bailey, C. G.; Kim, J.; Johnson, M. A. *J. Chem. Phys.* **1998,** *108,* 444-449.

[151] Kelley, J. A.; Weddle, G. H.; Robertson, W. H.; Johnson, M. A. *J. Chem. Phys.* **2002,** *116,* 1201.

[152] Hammer, N. I.; Shin, J.-W.; Headrick, J. M.; Diken, E. G.; Roscioli, J. R.; Weddle, G. H.; Johnson, M. A. *Science* **2004,** *306,* 675-679.

[153] Diken, E.; Robertson, W.; Johnson, M. *J. Phys. Chem. A* **2004,** *108,* 64-68.

[154] Neirotti, J. P.; Calvo, F.; Freeman, D. L.; Doll, J. D. *J. Chem. Phys.* **2000,** *112,* 10340-10349.

[155] Wang, F.; Jordan, K. D. *J. Chem. Phys.* **2003,** *119,* 11645-11653.

[156] Noga, J.; Bartlett, R. J. *J. Chem. Phys* **1987,** *86,* 7041.

[157] Raghavachari, K.; Trucks, G. W.; Pople, J. A.; Head-Gordon, M. *Chem. Phys. Lett* **1989,** *157,* 479.

[158] Earl, D. J.; Deem, M. W. *Phys. Chem. Chem. Phys.* **2005,** *7,* 3910.

[159] Metropolis, N.; Rosenbluth, A. W.; Rosenbluth, M. N.; Teller, A. H.; Teller, E. *J. Chem. Phys.* **1953,** *21,* 1087-1092.

[160] Fletcher, R. *Comp. J.* **1970,** *13,* 317-322.

[161] Franken, K. A.; Jalaie, M.; Dykstra, C. E. *Chem. Phys. Lett.* **1992,** *198,* 59–66.

[162] Lee, H. M.; Suh, S. B.; Tarakeshwar, P.; Kim, K. S. *J. Chem. Phys.* **2005,** *122,* 044309.

[163] Diri, K.; Jordan, K. D. Unpublished data.

[164] Wang, F. *A Drude model approach to disperion interactions in dipole-bound anions,* Thesis, University of Pittsburgh, 2003.

[165] McCunn, L. R.; Gardenier, G. H.; Guasco, T. L.; Elliot, B. M.; Johnson, M. A. *J. Chem. Phys.* **in press,** .

[166] Choi, T. H.; Jordan, K. D. *in preparation,*.

[167] Madarasz, A.; Rossky, P. J.; Turi, L. *J. Chem. Phys.* **2007,** *126,* 234707.